EXPERIMENTAL PROJECT REPORT

ON

Development and Characterization of 2mx2m Glass Resistive Plate Chambers

Submitted by
Neha Dokania

Under the guidance of
Prof .Naba K. Mondal

Development and Characterisation of 2m x 2m Glass Resistive Plate Chambers

Abstract:

The present work shows the design, development and characterisation of 2m x 2m glass RPC's .The details of the making of a 2m x 2m RPC, as a gas ionisation particle detector, the gas flow system using MFC (mass flow controller) and the electronic data acquisition system are discussed here. The trigger for the RPC is generated by a scintillator paddle telescope. The efficiency, noise rate, I-V characteristics and TDC plots are then obtained and studied for the RPC.

Introduction:

Glass RPC's have a long history dating back to the late 1970's [1].RPC array is a key component when it comes to the traditional function of muon detection. RPC's find use as the active elements in the tracking (iron) calorimeter which can simultaneously measure the energy as well as the direction of the charged particle. They are preferred over scintillators because of the following reasons: [2, 3]

1. They give a good position resolution and give good detection efficiency.
2. They can be made to have a large area but at a minimal material cost.[4]
3. These are easy to assemble and they possess simple read-out electronics.
4. They exhibit better time resolutions than scintillators and long-term stability.[4]

The glass RPC's have been proposed as the active element in the iron calorimeter detector for the India-based Neutrino Observatory. Single and double gap RPCs have found application in cosmic ray experiments, in high energy experiments as well as in astroparticle physics.

Principle of Operation of Glass RPC:

The resistive plate chambers described here are dc operated particle detectors whose sensitive element is a 2mm thick gas layer of Freon (134A), isobutane and SF_6 at normal pressure, under a uniform steady electric field of 4.5-5kV/mm generated by two parallel electrode plates of Asahi float glass with a volume resistivity of $10^{12}\Omega$-cm.When the gas layer is crossed by an ionising particle, an electric discharge is suddenly initiated by the liberated electrons. This discharge is quenched by the following mechanisms:

1. Prompt switching off of the field around the discharge point, due to the large electrode resistivity.
2. UV photon absorption by the quencher preventing secondary discharges from gas photo ionisation.
3. Capture of outer electrons of the discharge due to the gas with high electron affinity, which reduces the size of the discharge and possibly its transversal dimensions.

The duration of the discharge is typically ~ns. The relaxation time of the resistive electrodes plate is τ~2s.The large difference between these two characteristic times insures that during the discharge the electrode plates behave like insulators, so that only a limited area of ~0.1cm^2 around the discharge point remains inactive for the dead time of the detector.

Graphite painted high-voltage electrodes of surface resistivity 200-300kΩ/ cm^2, transparent to the electrical pulse originated in the gas; allow a capacitive readout through external pick up electrodes. These are copper strips about 3cm wide, facing the glass electrode (with thin mylar sheets in between for insulation against the high voltage).

Before,

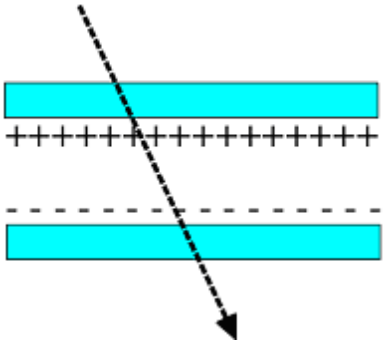

A passing charged particle induces an avalanche, which develops into a spark. The discharge is quenched when all of the locally ($r \sim 0.1 cm^2$) available charge is consumed.

Figure 1.a

After,

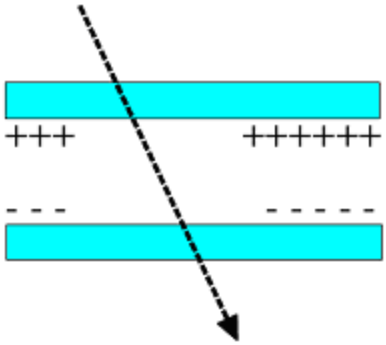

The electric field drops only around the streamer location, for a time proportional to the electrode resistivity. The discharged area recharges slowly through the high-resistivity glass plates

Figure 1.b

Modes of Operation:

There are two modes of operation for RPCs depending on the voltage of operation and gas composition used:

1. Avalanche Mode

Charged particles passing through the gaseous medium produce primary ionization. These ionized particles are accelerated by electric field thus producing secondary ionization by colliding with the gas molecules. This avalanche stops as the external field opposes the internal field due to ionization and the charged particles get collected on the respective electrodes. This mode operates at a lower voltage and typical pulse amplitudes are ~mV and hence amplifiers are required in the signal readout system.

2. Streamer Mode

In this mode of operation, the secondary ionisation continues until there is a breakdown of the gas and a continuous discharge takes place. This mode operates at a high voltage. Signal generated will be large and typical pulse amplitudes are ~100-200mV.

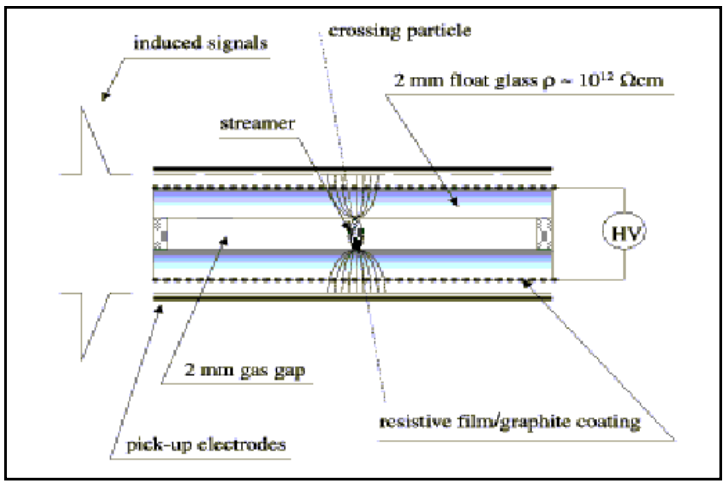

Figure 2.Schematic of a RPC in operation in streamer mode

A streamer mode is adequate for cosmic ray and low rate accelerator experiments, while an avalanche mode is required for high rate experiments such as CMS at LHC.

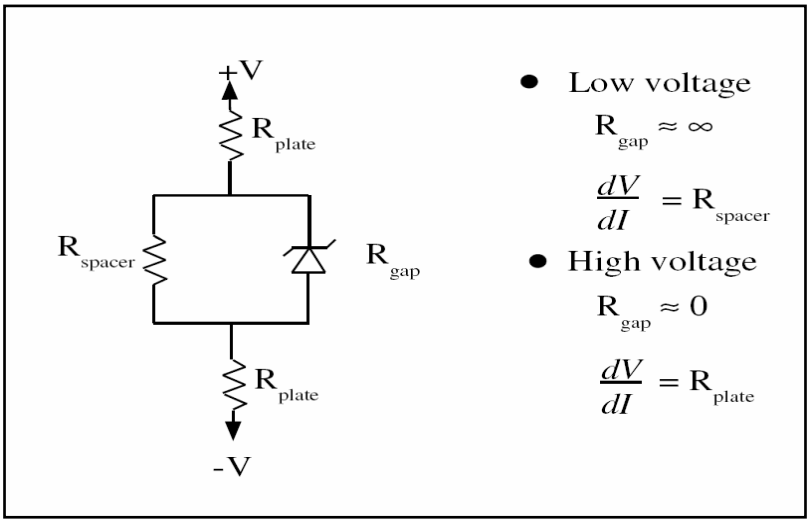

Figure3. Electrical Representation of RPC

Fabrication of 2m X 2m RPC:

Various stages involved in the fabrication of RPC are as follows:

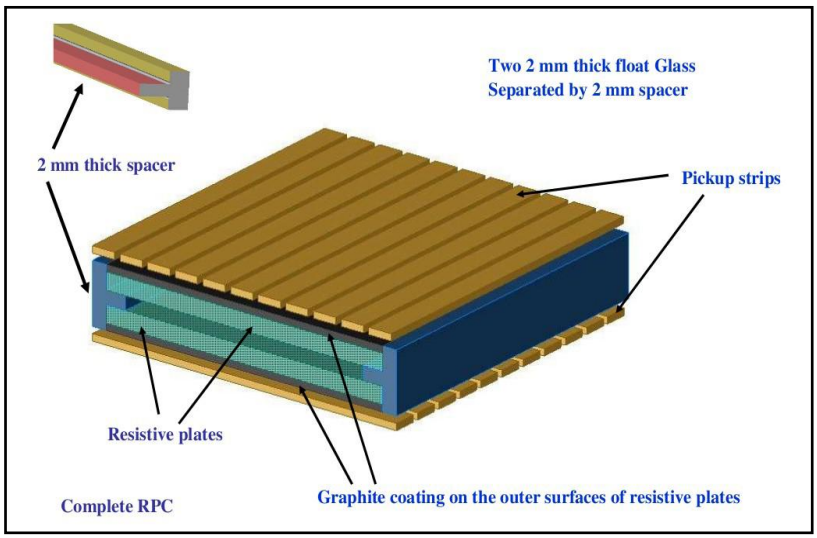

Figure 4.Structure of a standard single layer RPC

1. Glass Cutting and Cleaning

The Asahi float glasses (each 3mm thick) procured by local vendors are cut by diamond cutter to the appropriate size and the four corner edges are chamfered by a jig of right dimension to make a correct 45^0 angle. The glasses are thoroughly cleaned with alcohol followed by labolene and distilled water. After that the edge spacers, corner spacers (which are connected to the gas nozzle) and polycarbonate button spacers are also cleaned with alcohol. The glass edges are taped over with masking tape with 1 cm being masked or taped off on each side so as to prevent the conductive coating to be painted right up to the edge of the glass so that leakage of high voltage does not take place through the edge spacers

2. Conductive Coating

Conductivity of the glass is increased by coating one side of it with a mixture of dry colloidal graphite and industrial lacquer in a ratio of 1:8 using a spray gun. Once the surface is coated the masking tape is removed and the resistivity of both surfaces is measured using a resistance measurement jig (a copper and brass square about 17.5 x 17.5 cm^2). This layer serves two purposes: it is conductive enough to act as anode/cathode and it is

resistive enough to prevent itself from conducting away signal to the pickup strips so as to minimise the lateral spread. [11]

Surface resistance measurement:

The contour plots are obtained for five glass plates and two of them having fairly uniform surface resistance are selected for the construction of the RPC named as Al03. The surface resistance is found to be fairly constant and is about 100-200kΩ/cm^2.

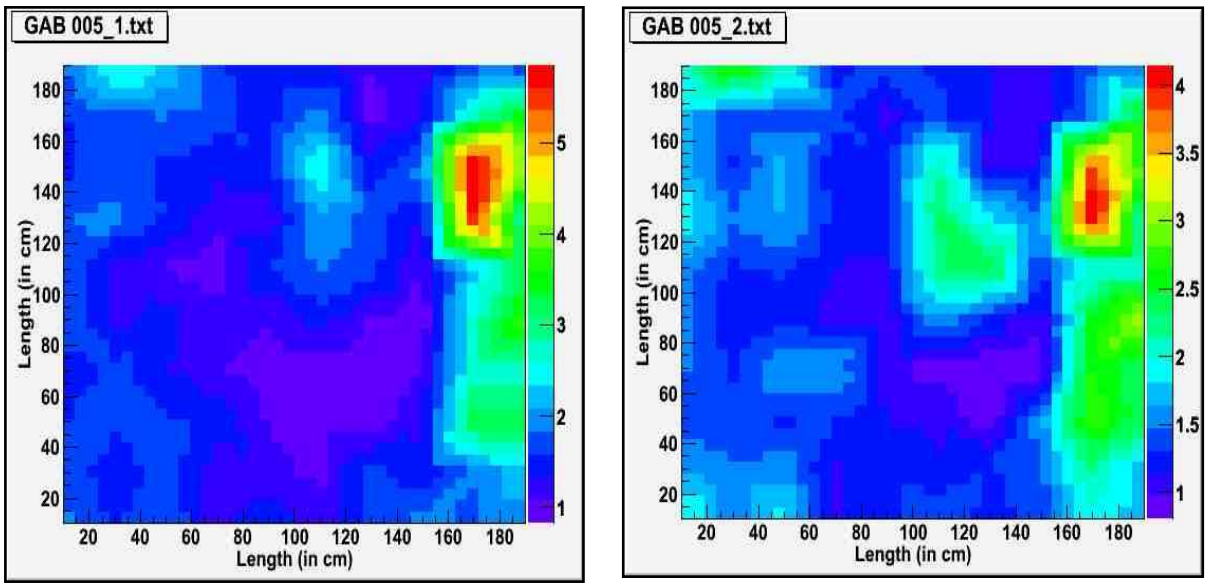

Figure 5(a),(b).Surface resistance along X-plane and Y-plane

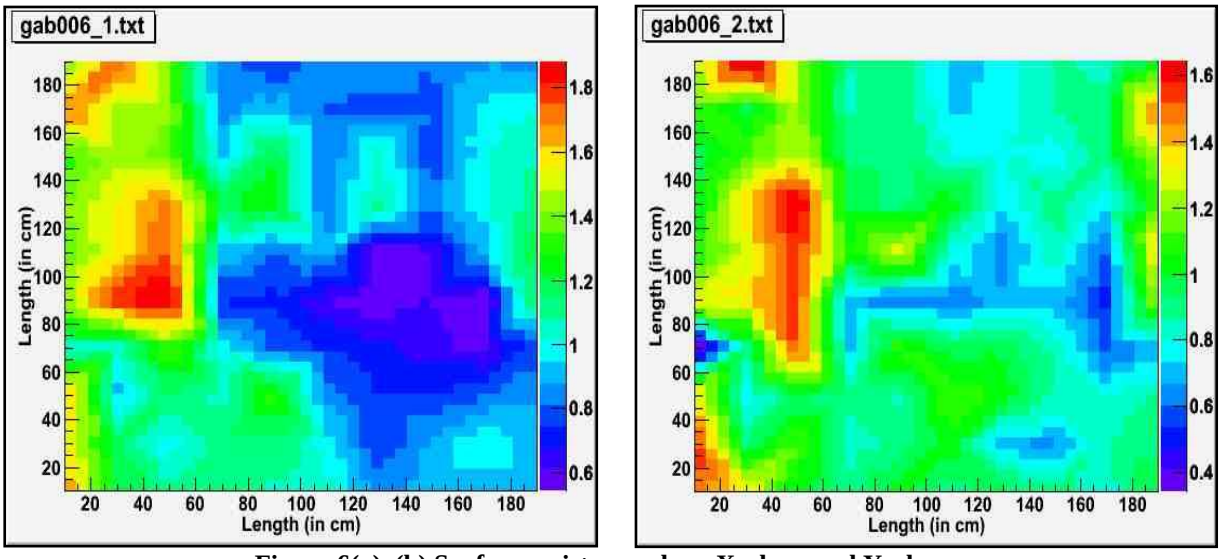

Figure 6(a), (b).Surface resistance along X-plane and Y-plane

There is variation in surface resistance near the edges due to non-uniform coating of graphite.

3. Gluing of Glass

The glue used is 3M Scotch-weld epoxy adhesive (DP 190) in a duo-pack cartridge. The button spacers (width ~1.8mm) are glued in a square array on top of the glass surface without the graphite coating. The glue comes out through the three holes of the spacers, and glue is again applied on top of the buttons. Then the other glass plate is placed on this array of spacers thus obtaining a gas gap of 2mm. To put a uniform weight throughout the 4m^2 area the whole set up is wrapped with plastic sheets and the air inside the plastic sheets is sucked slowly to create partial vacuum and a pressure equivalent to 5cm of water column pressure. The set up is left for six hours to fix the spacers. The straight edge-spacers are also designed such that the glass sits neatly within. There is a

1mm gap where the glue can be poured. The central protrusion is 2mm, thus supplying the required gap between glass plates. The corner spacers (gas nozzles) contain the gas inlet/outlet pipes. The glue is poured in the required gap and lead blocks are placed along the 4 sides to put the pressure and whole setup is left for one day, on the next day the same procedure is followed for the other side of the RPC.

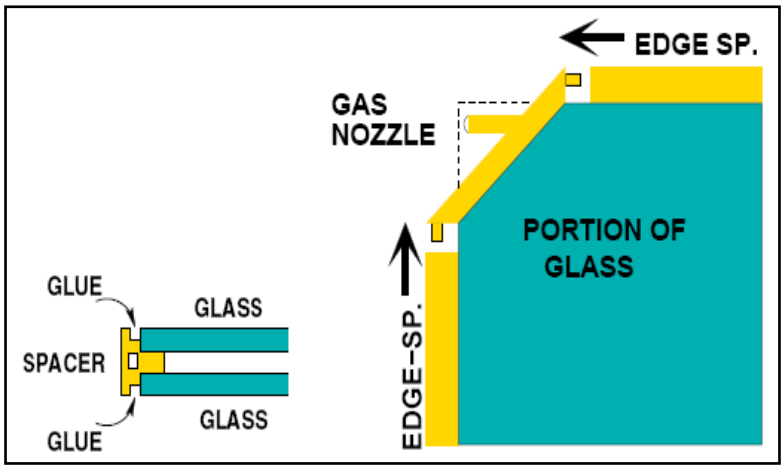

Figure7. Side-view and Top-view of Spacer

4. Gas Leak Test

To ensure against the gas leak (especially at the glued joints), a test is done by flowing Freon gas at slightly above atmospheric pressure and using a gas leak checker RIKEN GH-202F.Re-gluing is done on the edge spacers wherever a gas leak is detected.

5. High Voltage Cables

The high voltage is applied to the graphite layer by sticking on a copper tape and leads are then soldered on to the copper. Positive voltage is applied to one side and a equal and negative voltage to the other side, using a bi-polar high voltage DC supply (N471A), so that both see a common ground. The bi-polar connection is better than the unipolar since each glass surface sees only half the total voltage, thus decreasing the chances of HV leaks. Also it minimises the maximum absolute rating of the resources used e.g. HV modules and HV carrying cables.

6. Pickup Strips

The RPC is now sandwiched between two honeycomb pickup panels placed orthogonal to each other and then packed in an aluminium case. The pickup panel consists of 64 copper strips on one side and a layer of 5mm of plastic and aluminium(serving as a ground) on the other side. Each strip is machined to a width 2.8 cm and the gap between two adjacent strips is 0.2cm. Honeycomb panels are lightweight and provide adequate mechanical strength. Each strip is terminated with a 50Ω impedance to match the characteristic impedance of the strip. A layer of mylar of thickness 100μ is placed between the graphite layer and the pickup panel to provide insulation.

GAS FLOW SYSTEM:

The choice of filling gas for RPCs is governed by several factors: low working voltage, high gain, good proportionality and high rate capability. For a minimum working voltage, noble gases are usually chosen since they require the lowest electric field intensities for avalanche formation. The first ionization potential, the first Townsend co-efficient and the electronegative attachment co-efficient determine the avalanche multiplication, the presence and relative importance of photo production, the saturated avalanche range to the streamer mode. The gas mixture fixes the working mode of the RPC in 'avalanche' or in 'streamer' mode, resulting in different characteristics and performances.

Currently the RPCs are operating in the avalanche mode and hence the main component could be an electronegative gas, with high enough primary ionization production but with small free path for electron capture. The high electronegative attachment coefficient limits the avalanche electrons number. Here we use Freon (as eco-friendly R134A) which meets the above requirements. Polyatomic gases, often hydrocarbons, have a high absorption probability for ultra violet photons, produced in electron-ion recombination. This gas is known as quenching gas and limits the lateral charge spread. Here 'Isobutane' is used as the quenching gas. Finally SF_6 (Sulphur-hexafluoride) is used to control the excess number of electrons.

The system is designed for mixing four gases: Argon, Freon (134A), Isobutane and SF_6 by volumetric method. The gas mixing system consists of the following components:

1. Purifier Column: It contains Molecular sieve used to absorb moisture and purify it.
2. Mixing Unit: It is based on Mass Flow Controllers (MFC) and the flow of the gas is displayed in Standard Cubic Centimetre per Minute (SCCM).
3. Distribution Panel: 16 RPC's can be connected in parallel, which is achieved by "Flow resistors" viz. capillaries, which are 2m long and 200μ in diameter. These offers a resistance of 1/14th of a bar to the gas flow when the flow is about 6sccm.
4. Safety Bubblers: To take care of the back pressure exerted and protect the RPC's from over pressurizing.
5. Isolation Bubblers: It prevents back diffusion of air into the RPC and also indicates the flow of the gas. It also isolates RPC from the atmospheric pressure, thus acting as a buffer.
6. Exhaust Manifold: All the gas to be vented is collected in this manifold and a single output is provided to vent the used gas into the atmosphere. This manifold has a pressure sensor to indicate the pressure with respect to the room pressure.
7. Moisture Meter: Microprocessor based SHAW sensor meter to monitor the moisture content in the mixed gas. [6]

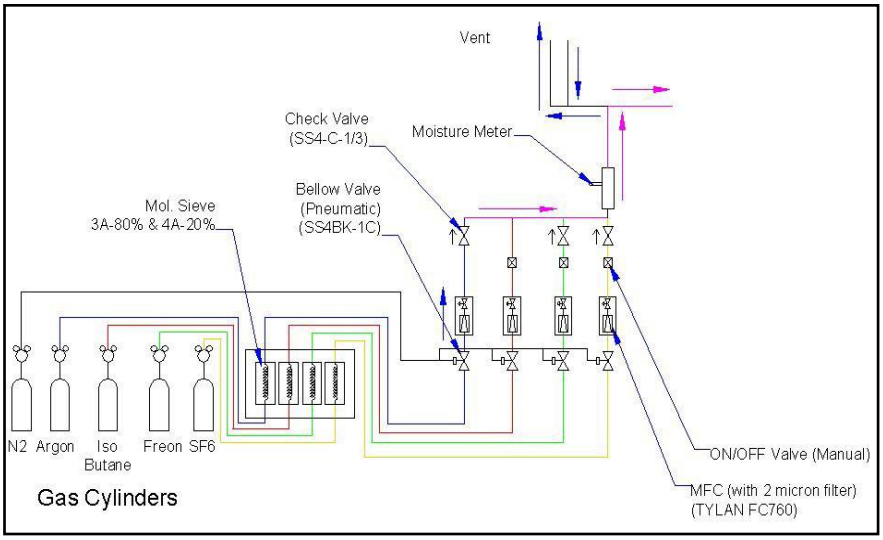

Figure 8.Block diagram of Gas Flow System

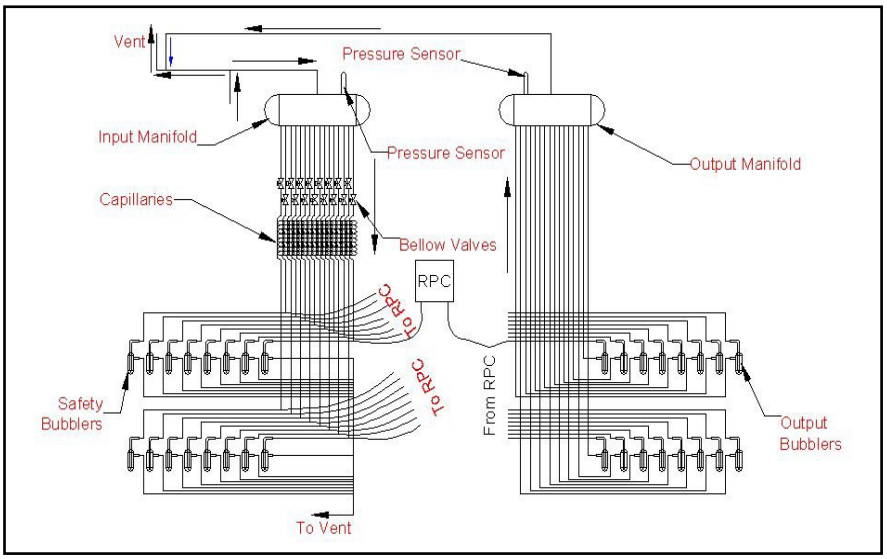

Figure9. Block diagram of Gas Flow System

The pressure of the gases to be mixed is controlled at the output of the cylinder itself by using two stage pressure regulators. The pressure set is 0.5 to 1 kg/cm^2 but as Freon (134A) and Isobutane gases are in liquid form low pressure input regulator of the order of 0 to 5 kg/cm^2 to be used, while for Argon and SF_6 the pressure is of the order of 25kg/cm^2**.**

On the display unit of the MFC, we have:

Gas constituents	Gas Flow (in SCCM)
Freon(R134A)	17.90
Isobutane	0.79
SF_6	0.07

There are two RPC's connected so each is getting 9.38 SCCM of total gas mixture.
The composition of the gases used thus is given below:

Gas constituents	Percentage
Freon(R134A)	95.42%
Isobutane	4.21%
SF_6	0.37%

Alignment of RPC in the laboratory:

To measure the efficiency of the RPC, firstly we ensure that the trigger pulse generated is solely due to the atmospheric muons. Six scintillator paddles are used to set a coincident circuit for this purpose, .i.e., a cosmic ray telescope with these scintillators. The telescope consists of 4 cosmic ray muon trigger paddles P1, P2, P5, P6 and two veto paddles P3, P4. The area of these scintillation paddles are 60×20, 60×20, 30×2,30×3 , 40×20, 40×20cm^2 respectively. The scintillation paddle gives out a signal when a cosmic ray muon or other charged particle passes through it. The geometry of the telescope using these paddles has been setup such that we define a window of about 30×2cm^2, for the cosmic ray muons to pass through the telescope as well as through one of the pickup strips of the RPC under test. Narrow paddles are used to define the telescope geometry precisely and veto paddles to prevent generation of triggers when a muon passes through the rest of the area of RPC which is not under study. The data from the RPC pickup strip is recorded whenever a cosmic muon generates a trigger signal through the logic $P_1 . P_2 . \overline{P_3} . \overline{P_4} . P_5 . P_6$ i.e., a trigger is formed when a muon passes through the paddles P_1, P_2, P_5 and P_6 and does not pass through the veto paddles P_3 and P_4.
The recorded data of the RPC is used for its characterization by finding its efficiency, time resolution and other parameters.

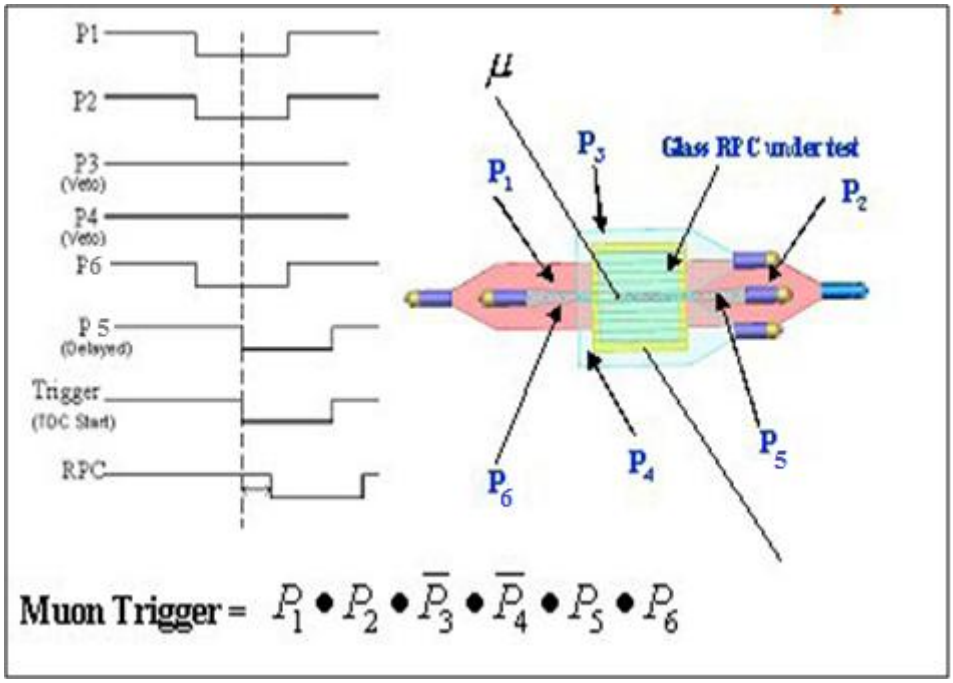

Figure10. Schematic of the RPC test setup

The analog pulses that come from the PMT's are converted to digital pulses through discriminators kept at a threshold of -30mV. P_1, P_2, P_5 and P_6 are ANDed and the veto paddles P_3 and P_4 are ORed. Scalars are added in every stage to monitor counting rates of these signals .The 4-fold pulse is NANDed with the veto to get 4fold x veto. The P_5 signal is delayed to take care of the jitter from the scintillation paddles which arises due to its finite time resolution. The pick-up strips of the RPC are connected to preamplifiers by twisted pair cables and to discriminators by coaxial cables and then output are taken to different channels of TDC with some delay. Trigger is taken from the middle strip of RPC (Main #32) and ANDed with 4fold x veto. Finally, 4fold x veto x RPC trigger is recorded.
Efficiency of RPC is defined as:

$$E = \frac{\text{4fold x veto x rpc}}{\text{4fold x veto}} \qquad ---(1)$$

The RPC pulses are connected to ADC before digitising and the 4fold x veto is given to the ADC gate to ensure that when TDC gives a START the ADC gate is also open at the same time.

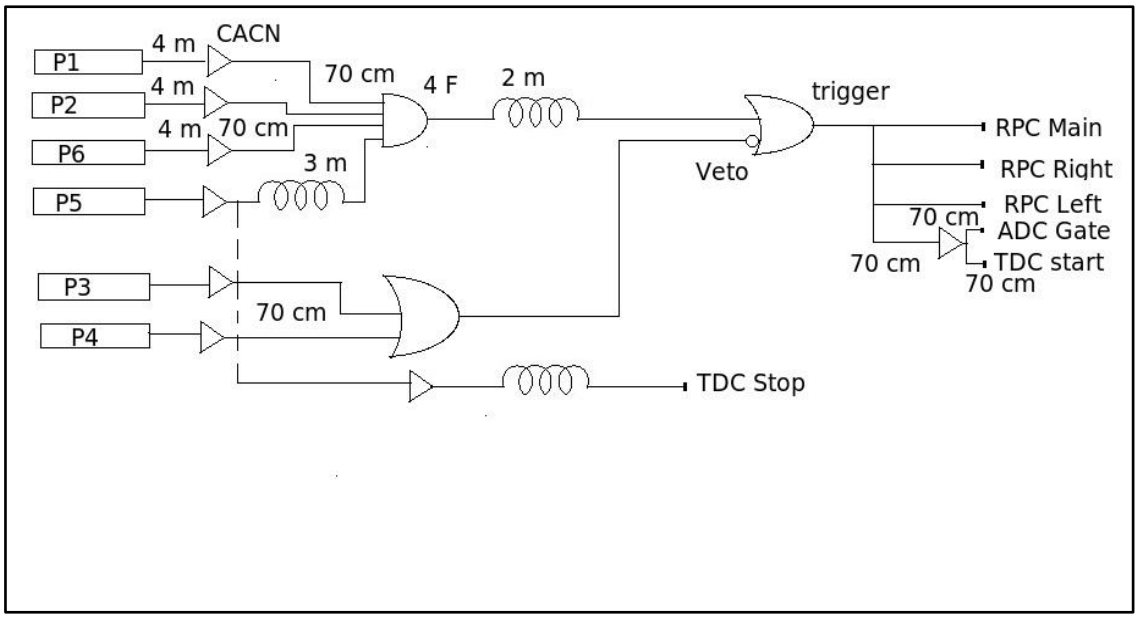

Figure11 (a). The circuit diagram for the trigger set-up

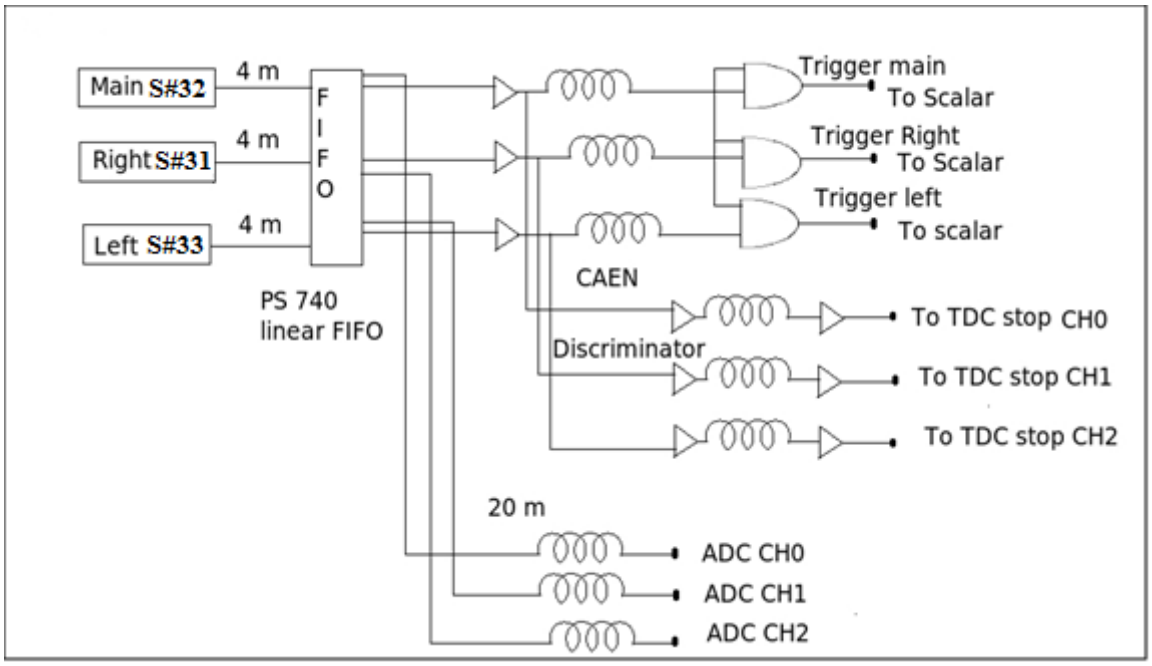

Figure11(b). The circuit diagram for the trigger set-up from the RPC

Electronic Data Acquisition System:

The entire signal processing and data acquisition system can be divided into the following modules:

- Front end electronics (16 channel analog front end and 32 channel digital front end).
- Trigger module.
- Signal routers (Trigger and TDC Router & Control and data Router).
- Back end DAQ system (Data and Monitor Control module & Data and Monitor Readout module).[5]

1. Front End Electronics

The signal from a pickup strip is passed through a pre-amplifier (gain70-80) and the output is fed to four 16 channel discriminator modules(Analog Front End).For channel-A, IC's 1597-1513 and for channel-B IC's 1595-1513 are used respectively. The signal crossing the set threshold in the discriminator generates differential ECL output. At present, the threshold is kept at -20mV. This section also generates the primitive trigger_0 logic. The

discriminator modules are connected to two 32 channel Front End Processing (FEP) module (Digital Front End) which converts the ECL i/p to TTL o/p and also generates trigger_1 signals. Both the DFE's work independently.

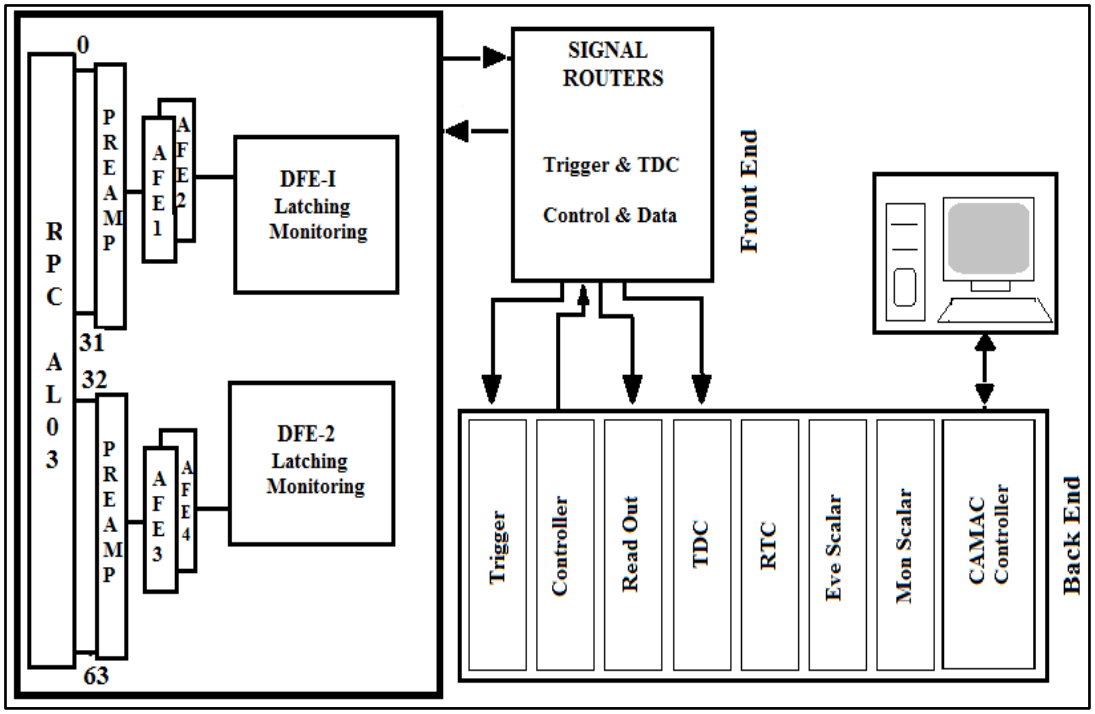

Figure12. Block Diagram of Electronics Set-up for x-plane of RPC

2. Trigger logic

The trigger logic picks up the event to be recorded. The basic principle of trigger generation is

M × N fold coincidence

where M is the layer coincidence of M consecutive signals out of 32 pickup signals and N is the no. of consecutive layers satisfying M fold layer coincidence. The M×N folds implemented are 1×5, 2×4, 3×3, and 4×2. Trigger is implemented in three stages. In the first stage i.e. trigger_0 logic, the shaped discriminator pulses from every 8th channel of 32 channels in the X-plane of RPC are logically ORed to get eight T0 signals. Similar signals are obtained for the Y-plane of each RPC. These eight T0 signals are logically ANDed to achieve the required Mfold triggers (T1 signals – 1F, 2F, 3F, 4F) in each layer. The trigger_1 logic is implemented in the Front End Processing (FEP) module using CPLDs. The M-fold signals (T1) from X-plane of all RPC layers are routed via Trigger and TDC Router module to the Final Trigger module in the CAMAC crate. The M×N coincidence logic (T2 trigger) is implemented in this module using T1 signals. T2 signals from X-plane and Y-plane are logically ORed to get the final trigger output which indicates the valid event to be recorded. The trigger generation rate is monitored with in-built scalars. All the triggers are maskable. [7]

3. Signal Routers

Trigger and TDC router receives the M-fold T1 signals and TDC signals from the FEP modules and routes them to the Final Trigger module and TDC module respectively. Control and Data Router receives control signals from the INO Controller module and routes them towards the FEP modules. It also receives data and feds the same to the Readout module.

4. Data Acquisition

A PC based data acquisition system is built using CAMAC standard modules in the back end which is connected to the front end with a fast serial link. The two main functions of the DAQ system i.e. Event Data Recording and Monitoring is controlled by the INO Controller module housed in the CAMAC crate. The Front End processing module of X and Y planes of all the RPCs are daisy chained into two groups for event data recording. At present no daisy chains are used for monitoring purpose and hence all the RPCs can be monitored

simultaneously. On a final trigger, CAMAC controller invokes an interrupt handler routine where INO controller initiates data transfer from front end modules in a bit serial mode via daisy chain and data is buffered in the Readout module for further CAMAC readout. A set of 40 signals are selected in each monitoring cycle by the INO controller, which invokes interrupt handler at pre-defined monitoring period (10sec) where rates of the selected signals are recorded and the next set of signals are selected for monitoring. The set of signals monitored in each cycle consist of 32 pickup signals of one RPC, 4 fixed frequency signals and 4 M-fold trigger_1 (1F, 2F, 3F, 4F) signals. The next 32 pickup signals of the same RPC are monitored simultaneously through the second DFE. The need is to record the event time, three dimensional interaction tracks and its direction in the detector. The event initiated by the final trigger records the Boolean status information of all pickup channels contributing to the track information. The relative time of interaction of track at each layer is recorded in the TDC which gives the directional information. [8]

Results:

1. The efficiency of the right (S31), main (S32) and left (S33) strips is calculated and plotted as a function of voltage applied. The main strip will show the maximum efficiency as the 2cm paddle was along the main strip.

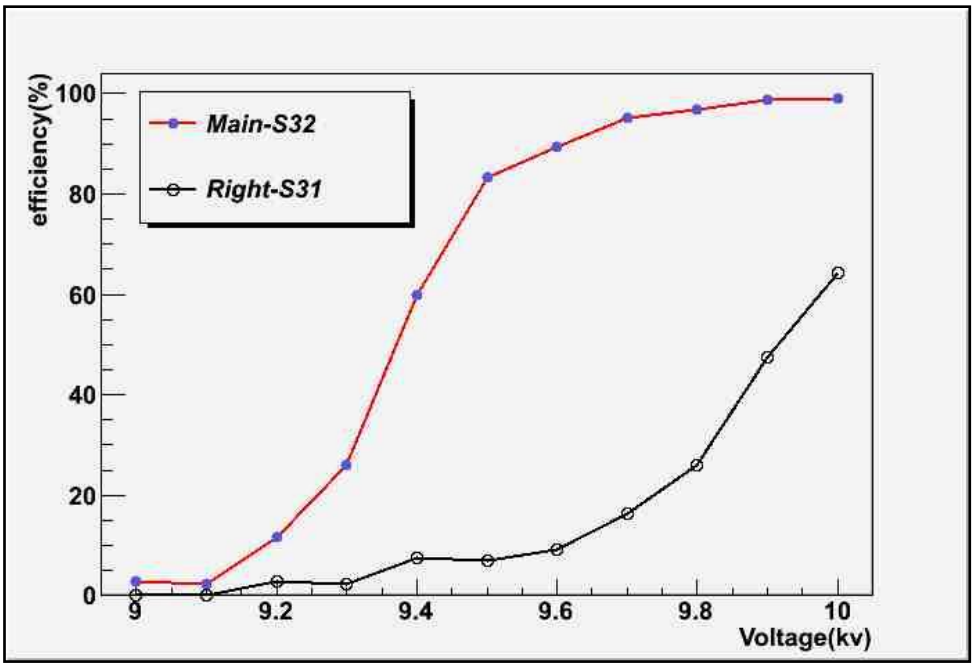

Figure 13.Efficiency vs. Voltage

The plateau region is achieved around 9.6kV (efficiency~95%) for the main strip. From the above graph, we see that cross-talks become prominent at higher voltages.

2. The I-V characteristics for both the glass plates of RPC AL03 are plotted.

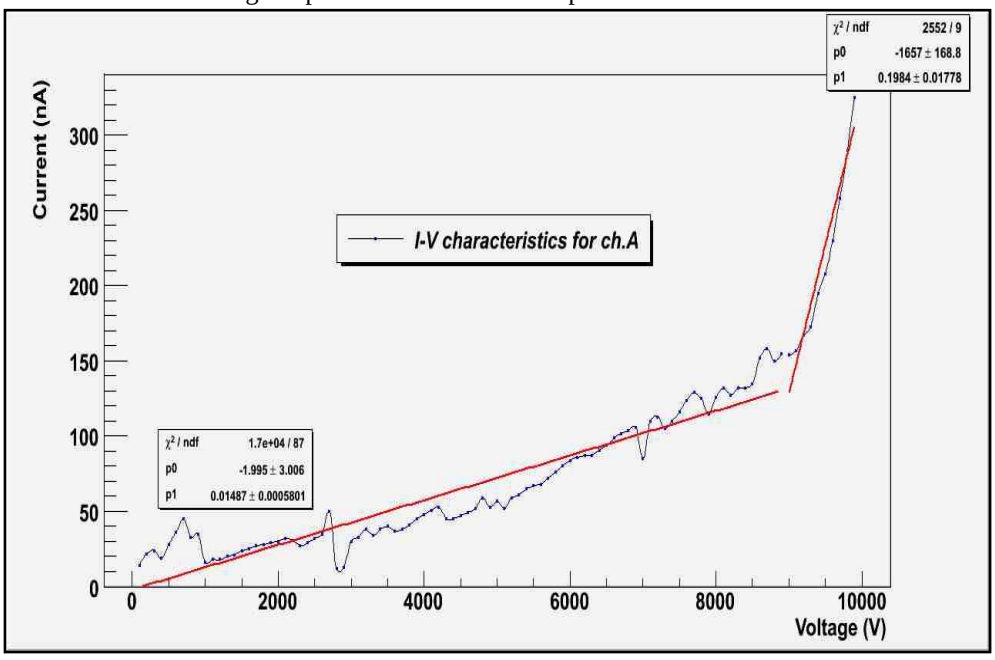

Figure14.Current vs. Voltage for channel A

Channel A correspond to the side on which negative voltage is applied and channel B on which positive voltage is applied.

From Figure 12, we get

Gap resistance = 67.2598 GΩ, at low voltages

Glass resistance = 5.04133 GΩ, at high voltages (above 9kV)

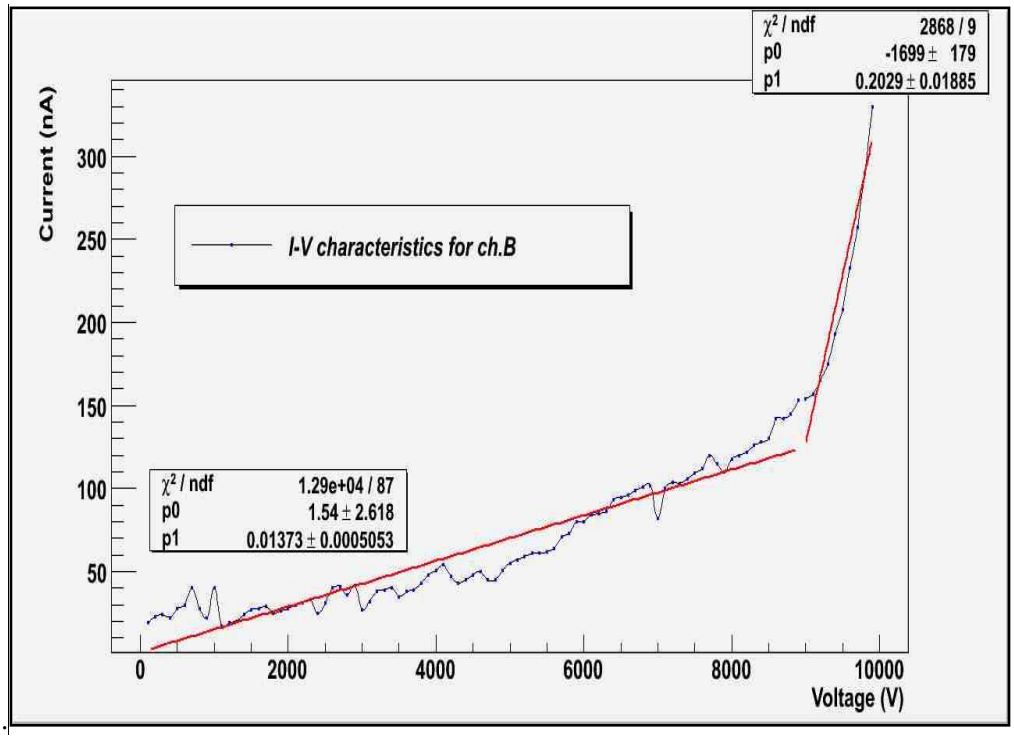

Figure15.Current vs. Voltage for channel B

From Figure 13, we get

Gap resistance = 72.8188 GΩ, at low voltages

Glass resistance = 4.9283 GΩ, at high voltages (above 9kV).

3. The noise rate as a function of voltage and the TDC plot are obtained at 9.6kV for the RPC AL03.

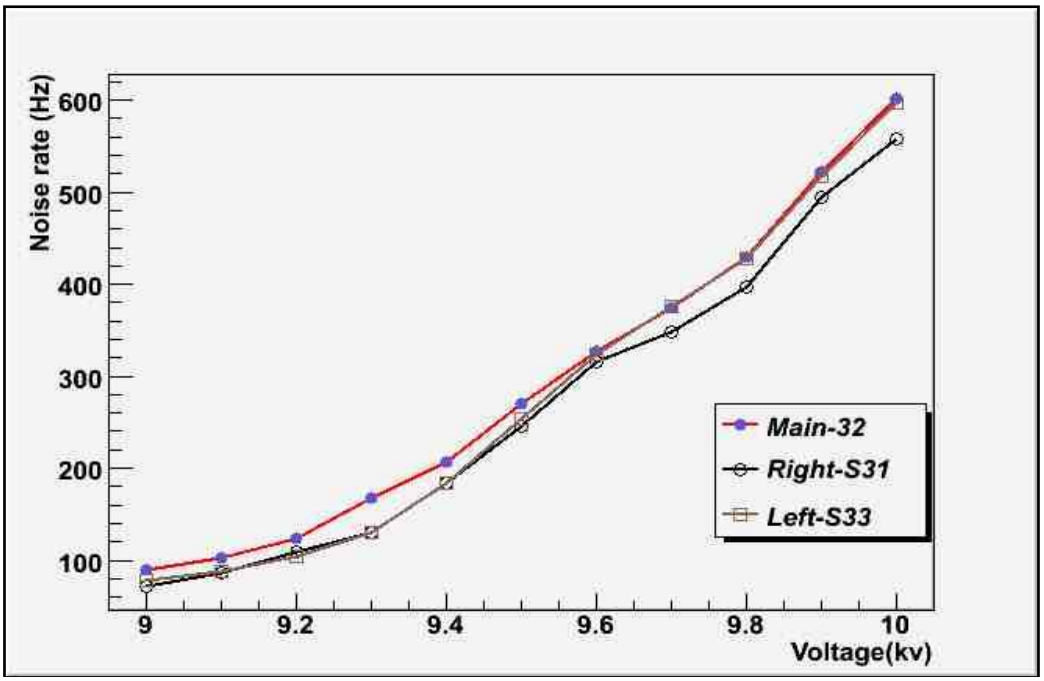

Figure16.Noise rate vs. Voltage

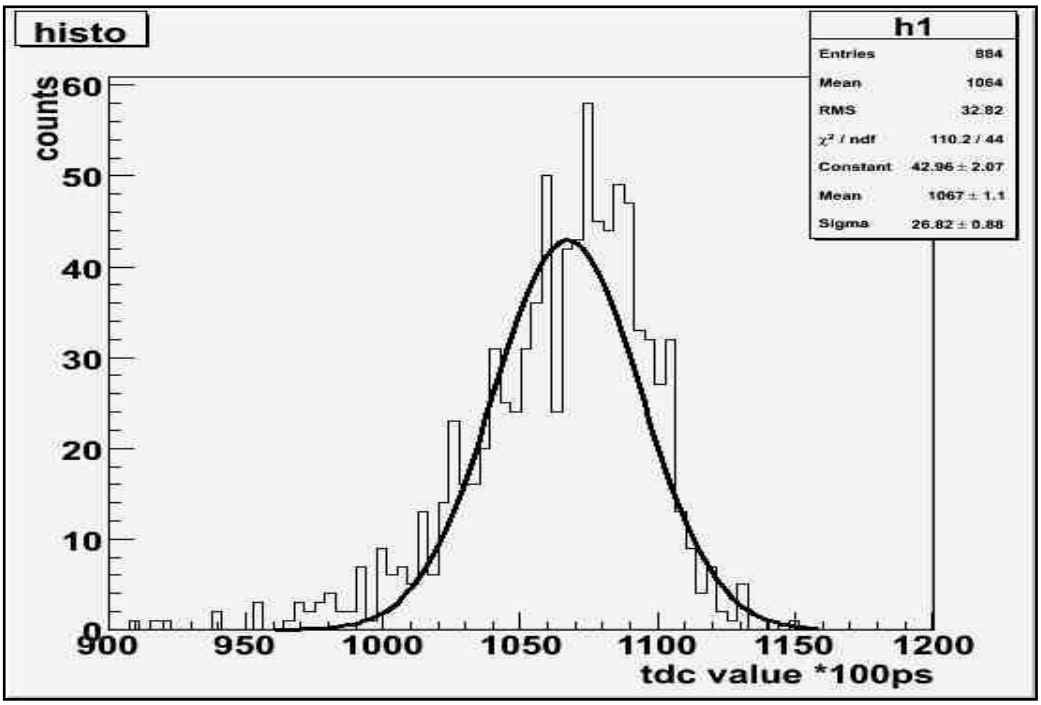

Figure17.TDC plot at 9.6kV

The time resolution of the RPC is $\sigma = 2.7 \pm 0.1$ ns.

Conclusions:

The construction of 2m x 2m RPC AL03 is successfully completed and it is operating in the avalanche mode with an efficiency of about 95% at a voltage of 9.6kV.It is characterised and the time distributions are also studied.

Acknowledgement:

I am highly indebted Prof. N.K. Mondal for providing such a golden opportunity to work in the INO RPC Lab. I would like to express my sincerest gratitude to Dr B. Satyanarayana for explaining the DAQ system so lucidly. I am also thankful to Shri S.D. Kalmani who helped us on the gas flow system related issues. I would also like to mention Shri R.R.Shinde , without whose guidance completion of this project would not have been possible. Md. Salim helped in using the ROOT software for making the plots. Lastly, I would like to thank my colleagues Moonmoon, Animesh and Mathi for their patience and full co-operation. It was a thoroughly learning and overwhelming experience.

References:

[1] Yu N.Pestov, G.V.Fedotovich, Preprint IYAP-77-78, Slac Translation, 184 (1978); G. Battistoni et al., Nucl. Instr. and Meth. 152, 423 (1978); G.Battistoni et al., Nucl. Instr. and Meth. 176, 297 (1980)
[2] Daniel Marlow, Princeton University, Seminar at Rice University (1999)
[3] G.Battistoni et al., Nucl. Instr. and Meth. 202, 459 (1982)
[4] M.Anelli, G.Bencivenni, G.Felici, L.Margo, Nucl. Instr. Meth. A 300, 572-574 (1991)
[5] S.S.Upadhya, "Conceptual design of DAQ system for a prototype detector".
[6] S.D.Kalmani, N.K.Mondal, B.Satyanarayana, P.Verma, "Online gas mixing and multi-channel distribution system".
[7] B.Satyanarayana, "ICAL electronics and DAQ schemes".
[8] B.Satyanarayana, "Electronics for the INO ICAL detector".
[9] B.Satyanarayana, "Commissioning of ICAL prototype detector electronics".
[10] S.S.Upadhya, "Electronics and DAQ system for INO prototype detector".
[11] V.M.Datar, S.Jena, S.D.Kalmani, N.K.Mondal, P.Nagaraj, L.V.Reddy, M.Saraf, B.Satyanarayana, R.R.Shinde, P.Verma, "Development of Glass Resistive Plate Chamber for INO experiment".
[12] S.Biswas, "Resistive Plate Chambers for experiments at India -based Neutrino Observatory".

Measurement of Mean μ-Lifetime

Neha Dokania*

*INO Graduate Training Programme, TIFR

Abstract:

The average muon lifetime is determined in the experiment by stopping muons in a plastic scintillator, where they subsequently decay into electrons. From these stopping muons we get two pulses: one from the entry of a muon and a second one a short time later from the electron arising from the muon decay. The time delay between the two signals is measured for a large number of decays and produces an exponential distribution. To get the lifetime we measure the decay constant which on a logarithmic scale is 1/slope of the line.

Introduction

Muon is an elementary particle and one of the fundamental constituents of matter. Muons belong to the family of leptons (second generation) together with electrons and taus. They behave much like electrons but are heavier than them, with mass of about 105.7Mev/c^2, carry one unit of fundamental charge and are unstable. Muons participate in electromagnetic and weak interactions and are not subjected to strong interactions. On passing through matter, muons (or anti-muons) decay spontaneously via weak interaction into a neutrino-anti-neutrino pair, and an electron (or positron), as shown below:

$$\boldsymbol{\mu^- \rightarrow \nu_\mu + e^- + \overline{\nu_e}}$$

$$\boldsymbol{\mu^+ \rightarrow \overline{\nu_\mu} + e^+ + \nu_e}$$

Muons can also be captured by nucleus. They are highly penetrating particles .Owing to their large mass; emission of Bremsstrahlung radiation is limited on its passage through matter.

Cosmic Muons

Most of the primary cosmic rays consist of protons (92%) , alpha particles(7%) and some heavier nuclei(1%). To produce muons, primary cosmic ray protons interact in the upper atmosphere with atmospheric nuclei like oxygen and nitrogen to produce secondary particles like pions. These pions with a mass 273 times that of the electron are not stable and have a lifetime of about 10^{-8}secs. They decay "radioactively" into muons .Neutral pions decay into a pair of gamma rays.The muons that are so produced, due to their longer lifetime (10^{-6}secs) and almost complete absence of nuclear interactions, are the principle components of penetrating particles produced by cosmic rays that are observed at sea levels; the sequence of events is illustrated in fig.1.

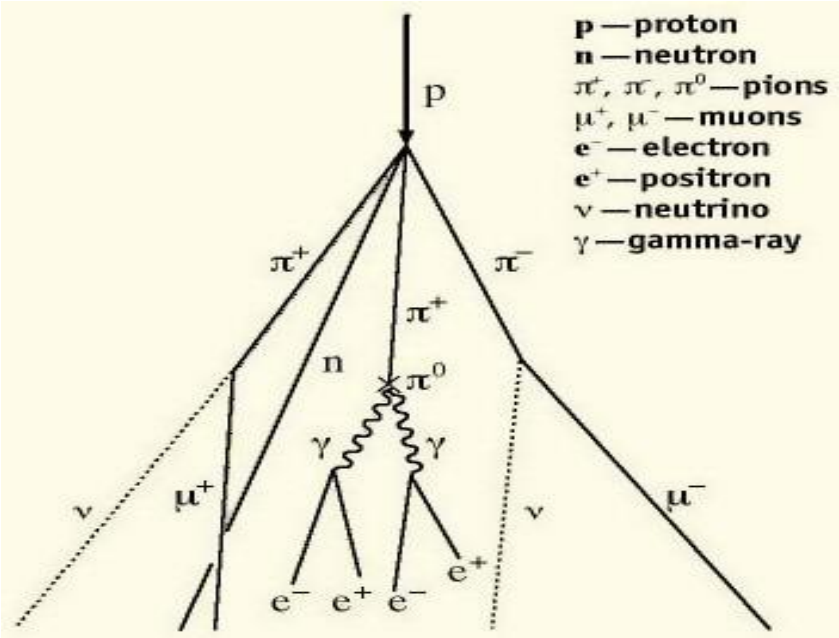

Figure 1. A typical interaction between a cosmic ray proton and an atmospheric nucleus.

Many of the new particles formed are short lived and do not survive to reach sea level but muons are detectable at ground level. The total secondary flux at sea level is $1cm^{-2}min^{-}$ .Roughly 75% consists of positive and negative muons and only 25% electrons and positrons.

If the mean lifetime of the free muons is a few μs then according to classical physics, they should travel a few hundred meters when travelling at the speed of light after being created in the upper atmosphere and many fewer than that indicated above would be expected to reach the ground. Relativistic time dilation effect can explain this.

We know that,

$$t = \frac{t'}{\left(1 - \frac{v^2}{c^2}\right)^{\frac{1}{2}}} = \gamma t'$$

where, t is the time measured in the laboratory system,
t' is the time measured in the rest frame of the system,
v is the velocity of the system, and
c is the speed of light.

Thus to an observer on Earth, the muons have a lifetime equal to γt'. Hence if v=0.99c the average distance travelled by muons as measured by an observer on Earth is 4712.4m for t'=2.2μs.

Aim

The aim of this experiment is to determine the average muon-lifetime. This is accomplished in the experiment by stopping the muons in a plastic scintillator, where they subsequently decay into electrons.

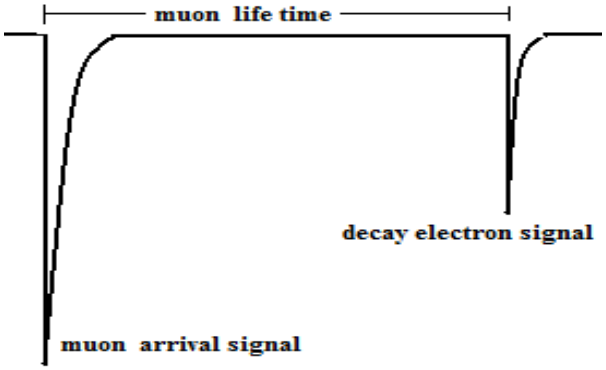

Figure 2: Output of PMT

A short light pulse is produced by the stopping muon which is detected and amplified by a PMT .When the muon decays a second pulse is produced by the emitted electron or positron.The signals for the PMT are fed into an electronic circuit which determines the time delay between the two pulses. The circuit is connected to a PC which is used to read out the data. The distribution of the muon spontaneous decay is governed by the general radioactive decay law,

$$N = N_0 e^{\frac{-t}{\tau}}$$

The average muon- lifetime is then determined by fitting exp(-t\$\boldsymbol{\tau}$) to distribution of the time intervals between entry of muon stopped in the scintillator and their subsequent decay. Hence for the experiment only those muons are considered which slows, loses all their kinetic energy and stops in the detector and decay subsequently.

Experimental Setup

The basic components of the experimental set-up are:

- Plastic scintillator
- Photomultiplier tube
- Time measuring circuit
- PC

1. Plastic scintillator: We are using a plastic scintillator (refractive index =1.58) of dimensions (24cm x 24cm x 14.5cm).Plastic scintillator are characterized by a relatively large light output and a short decay time of the order of a nanosecond. This makes the material well suited for fast timing measurements. It is wrapped carefully in highly reflecting (Tyvec)

paper to minimize the light loss and then wrapped in Tedlar sheets to prevent the ambient light from entering the scintillator and hence minimizes stray scintillation. When a charged particle like muon passes through this detector, it loses some of its kinetic energy by ionization and atomic excitation of the scintillator molecules. The de-excitation of molecules then produces radiation near the blue and below UV region of electromagnetic spectrum.

2. Photomultiplier tube: The plastic scintillator is directly coupled to the PMT. A 2 inch diameter PMT with 21 pin base (type 9807B, Electron tubes Ltd. manufactured) is used to convert the light signals obtained from scintillator into amplified electrical signals. The incident photons from the scintillator strike the photocathode of the PMT producing photo electrons, these electrons are directed by focussing electrode on Dynodes where secondary electron emission takes place. The final charges are accumulated and then collected at the anode, which gives rise to a sharp and strong electrical output.

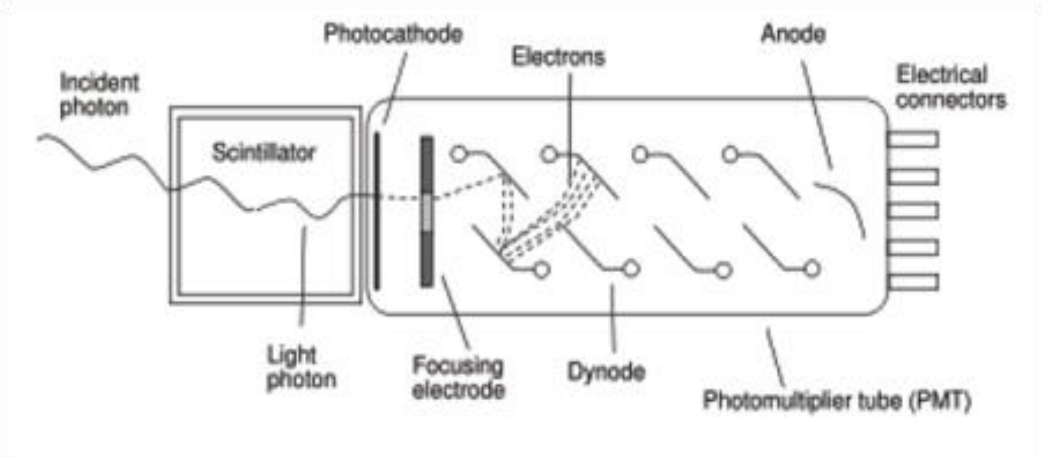

Figure 3: Schematic of a PMT coupled to a scintillator

The PMT base is applied a high voltage of 1.7kV by means of high voltage dc to dc converter (E20-HVDCDC).Negative pulses with a rise time of few nanoseconds are obtained at its output.

3. Time measuring circuit: The main counter circuit mainly consists of comparator, flip-flops, counters, oscillator, latches, a buffer IC and a Standard Parallel Port interfacing with the computer where the data is recorded.

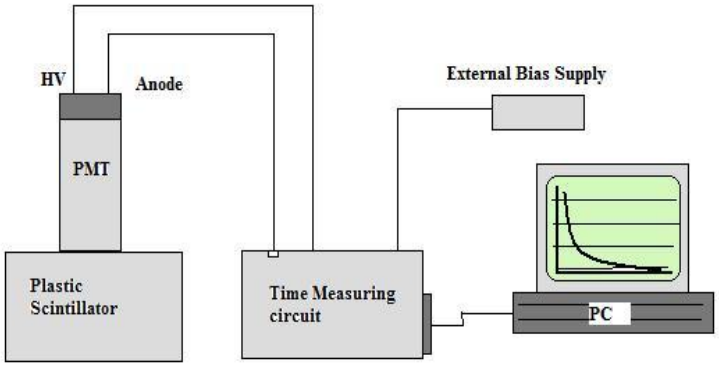

Figure: 4 Schematic diagram of muon life time measurement counter circuit

The Electronic components used are listed below:

IC details:

IC NAME	DESCRIPTION
LM360(8 pins)	Comparator
74LS74(14 pins)	D-Flip Flop
74LS161(16 pins)	4-bit Counter
74LS541(20 PINS)	Buffer
74LS11(14 pins)	And gate
74LS04(14 pins)	Not gate
7805(3 pins)	Positive voltage regulator
7905(3 pins)	Negative voltage regulator
DB103(4 pins)	Bridge rectifier

A crystal oscillator of frequency 10MHz is used to generate the clock for both LSB and USB counters, thus giving the resolution of 0.1μs.

Electronic Circuit Operation: The reset switch is pressed before starting the experiment to ensure that all F-F's are in clear states through the AND gate (IC 74LS11).Hence initially both flip flops are in a cleared state, waiting for a start pulse from the PMT signifying the entry of a muon. In clear states the Q o/p of the F/F's are set to low while $\overline{Q}$ is set to high. The D of the first F/F is set to high and the clock of the second F/F is high. However the o/p of the second F/F does not change state because of the clear signal.

The signal is not free of noise and the actual signal rides over this noise. If present, the noise can trigger the counters giving spurious results. Hence the negative pulse from PMT is fed to a comparator (IC LM360). It filters out the noise by allowing only those signals to generate high logic pulse whose levels are above the threshold voltage, - 42mV (in the present case), set at the non-inverting terminal of the IC. The output of the comparator is positive high (since, the negative input signal is fed to the inverting terminal) logic pulse of 5 volts.

The comparator output is then fed to the clock pin of the first F/F (IC 74LS74).The Q o/p of this positive edge-triggered F/F goes high which enables the 4-bit LSB counter (IC 74LS161) and it starts counting at 10 MHz. The $\overline{Q}$ o/p goes low which is taken to the clock input of the second F/F. Hence its $\overline{Q}$ remains high. When the LSB counter reaches binary 15 ,the RCO pin goes high which enables the USB 4-bit counter(IC 74LS161) and it starts counting at 10MHz.

If the muon decays into an electron, a second pulse comes from the PMT, the Q o/p of the first F/F goes low and the LSB counter is stopped. It's $\overline{Q}$ o/p goes high and makes the clock i/p of the second F/F high. Thus the $\overline{Q}$ o/p goes low of the second F/F, is read by the interfacing program as the time when the data from the buffer (IC-74LS541) is to be read. And the signal is sent to the BUSY pin of the PC parallel port. When the PC receives the BUSY signal, the DATA_STROBE LINE is pulled low to enable the data buffer. The data buffer passes the count from the counter to the PC. After the PC has read the data, DATA_STROBE is taken high and the RESET line is pulled low for a few µs. This RESET signal clears the F/F's and counter ready for the next signal from the PMT. The interfacing program writes the total number of counts and the time and date of writing of file.

If the muon passes through the scintillator without decaying, the USB counter reaches 255, i.e., a second pulse is not received within 25.5µs, and its RCO pin goes high. This is inverted through a NOT gate(IC 74LS04) to clear the counters and F/F's, and to wait for the next pulse from the PMT.

The program is run till required number of data points for good statistical measurement is obtained (48500 data points in the present case).

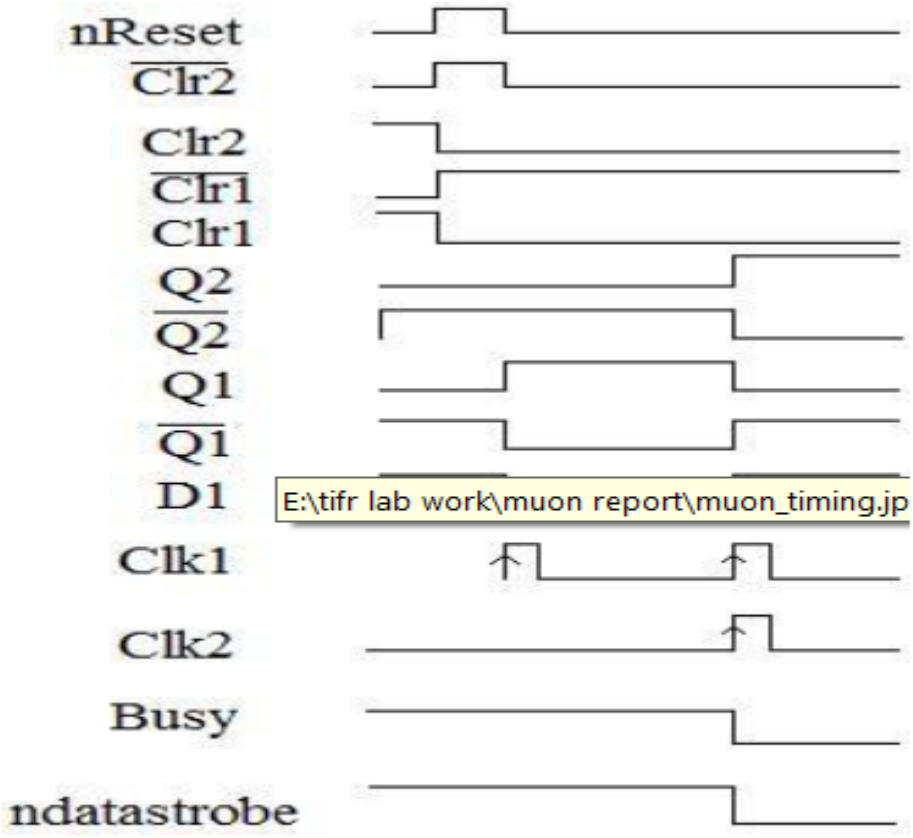

Figure 5: Timing Diagram for the signals

The timing diagram shown above in fig.5 gives the output waveforms for the flip flops with respect to the clock inputs. (Clr1,Q1,D1,Clk1 correspond to the first flip flop and Clr2,Q2,D2,Clk2 correspond to second flip flop.)

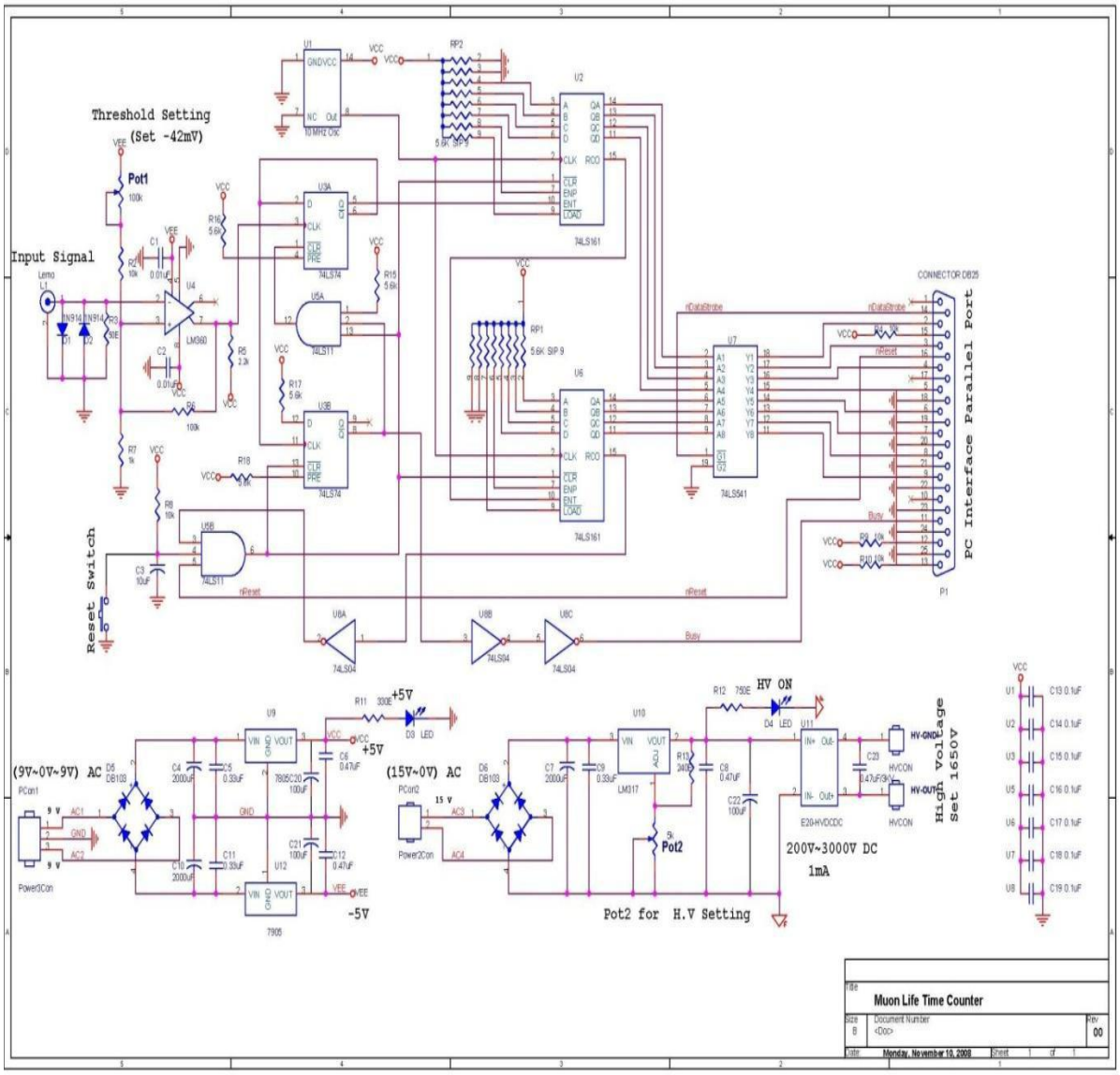

Figure 6.Electronic circuit diagram

The two circuits shown below the main circuit in Fig.6 employs the voltage regulators for providing voltages to IC's (+5 volts and -5 volts) and PMT base (rated1700V)

Analysis

The file saved contains a column of data which are the different time intervals for each muon decay, i.e., the time lag between the start event and stop event. The analysis of data requires fitting of data with appropriate exponential functions, taking background events into account. For the distribution, the sampled data is sampled and the events binned and fitted. The background events are random coincidences of signals not arising from muon decays. These are mainly due to natural radioactivity, through-going muons and PMT after-pulses. The background events which are produced due to start from one muon and stop from another

will be negligible as the flux reaching down sea-level is very small when compared to the 25.6μs window employed for counting.

If the background for the data is assumed to be constant over a period of time , then the measured decay spectrum follows the law:

$$N = N_0 e^{\frac{-t}{\tau}} + b$$

where, N_0 is the normalisation parameter,
b is the number of background events per time bin.

The data is fitted with the above function using ROOT and the fitting parameters obtained are:
$N_0 = 855.9 \pm 9.8$
$b = 9.54 \pm 0.27$
$\boldsymbol{\tau}$ = (2.19±0.02)μs

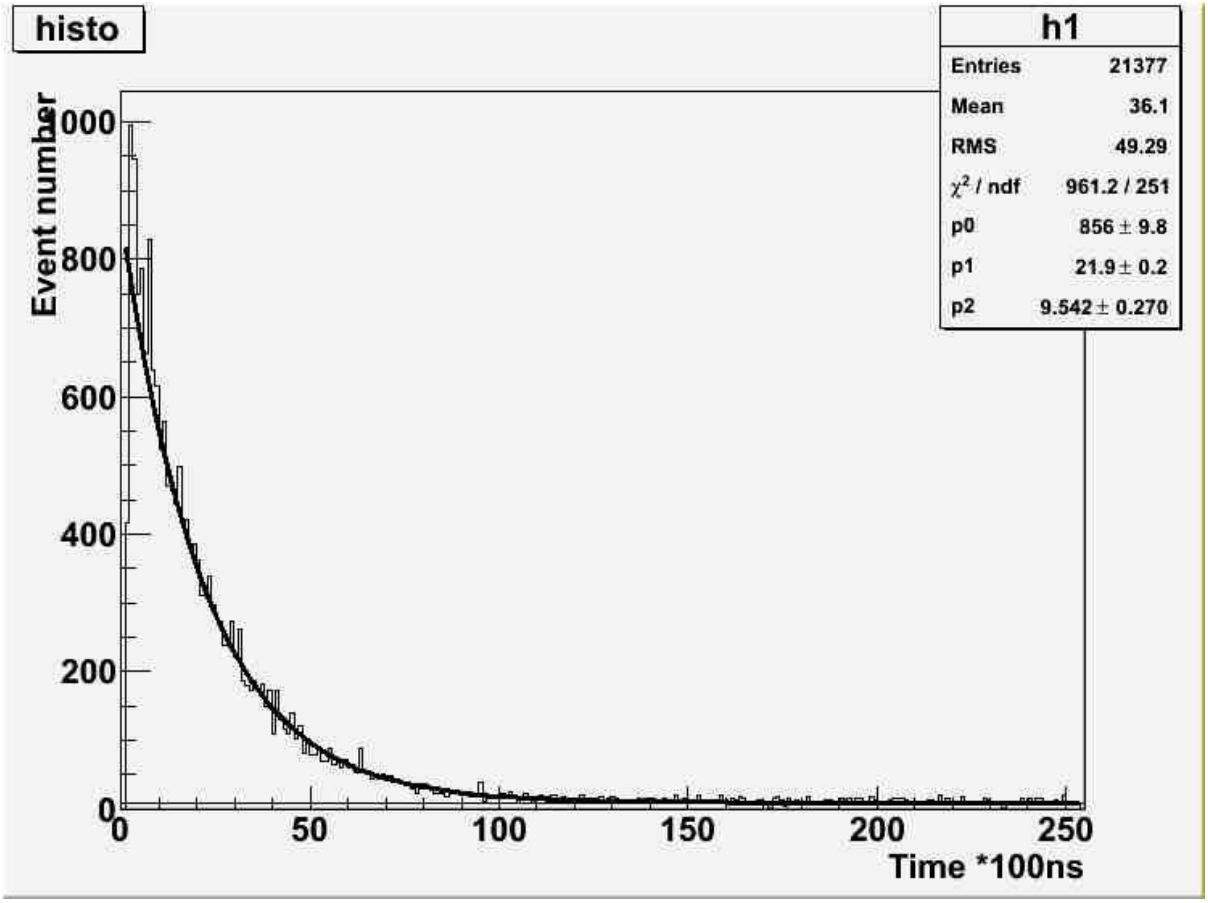

Figure 7: Muon lifetime distribution with background

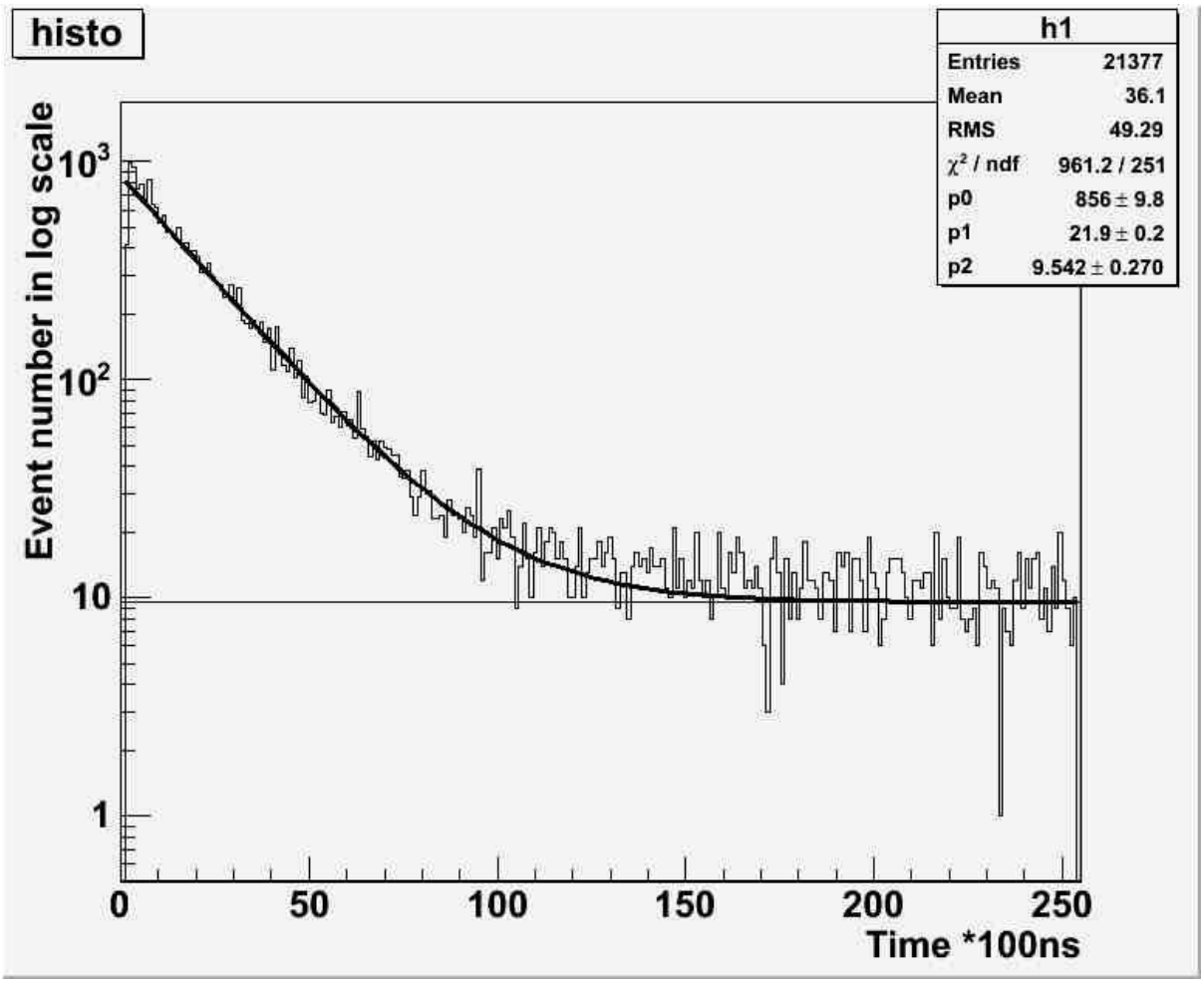

Figure 8: Muon lifetime distribution with background taking event numbers in Log scale

Hence the average muon lifetime is obtained as:

$$\tau = (2.19 \pm 0.02)\ \mu s$$

Fermi Coupling Constant: The universal constants for a process provide a tool to validate experimental results. The Fermi Coupling Constant plays a key role in all precision tests of

electroweak model standard model .In the theory of muon decay , which is an electroweak process, the expression for average lifetime of muon is given as:

$\boldsymbol{\tau} = 192\ \pi^3 / G_F^2 m_\mu^5$

By putting the above value of $\boldsymbol{\tau}$ in the following relation,

$G_F^2 = 192\pi^3 / \boldsymbol{\tau}\ m_\mu^5$

The value of G_F in natural units is obtained as:

$G_F = 1.16533 \times 10^{-5} GeV^{-2}$

where m_μ is taken as 105.66 MeV.

References

1. *"Radiation detection and measurement" by G.F.Knoll*
2. *http://root.cern.ch/*
3. *J.Santos, J.Augusto, A.Gomes, L.Gurriana, N.Laurenco, A.Maio,C.Marques, J.Silva, "The CRESCRE Muon's Lifetime Experiment".*
4. *Dr. F.Muheim, "Muon Lifetime Measurement".*
5. *IC datasheets of Fairchild Semiconductor, Motorola, ST Microelectronics and National Semiconductor.*
6. *"Introduction to elementary particles" by D. J. Griffiths*

Experimental Project Report

on

Measurement of "speed of light" using $LaBr_3$ scintillator detectors

Submitted by

Neha Dokania

Under the guidance of

Prof. Vandana Nanal

India based Neutrino Observatory
Tata Institute of Fundamental Research
Mumbai 400 005

[31st March 2010]

Measurement of "speed of light" using $LaBr_3$ scintillator detectors

Abstract:

The present experiment aims to measure the speed of light with two 511KeV photons from positron annihilation obtained from a 20μCi Na-22 source. The photons are detected by two $LaBr_3$ scintillation detectors and time difference is measured as a function of distance (100cm to 600cm) .The speed of light is determined to be (30.018±0.028)cm/ns, which is very close to the measured value of 29.99792458cm/ns[3].

Introduction:

Scintillation spectrometers are widely used in detection and spectroscopy of energetic photons (γ-rays). These detectors are commonly used in nuclear and high energy physics research, medical imaging, and diffraction. Important requirements for the scintillation crystals used in these applications include high light output, high stopping efficiency, fast response, low cost, good linearity, and minimal afterglow.

In this experiment, cerium doped halide inorganic scintillator $LaBr_3$ is chosen because of its balance of high collection efficiency, very high light output (~6 x 10^7 photons/keV), and fast principle decay constant (30ns)[1] and good timing resolution. With resolution of approximately 3 percent at 662keV, lanthanum bromide scintillator offer a substantial improvement over sodium iodide (NaI[Tl]) scintillator, whose resolution is approximately 6-7 percent in comparable sizes. But the lanthanum halide scintillators have a few drawbacks of their own: internal radioactivity and a low-energy response that results in the resolution being lower than that of NaI(Tl) below approximately 100keV. The internal radioactivity is due to naturally occurring radioisotopes ^{138}La and ^{227}Ac [2] .Also the time resolution of $LaBr_3$ is better than NaI and BaF_2.

Na-22 decay mechanism:

The ^{22}Na decay (half life -2.7 years) occurs by one of two independent mechanisms as shown in Figure.1.

(1) β^+ Decay:In each of the two beta decay branches

$$^{22}Na \longrightarrow {}^{22}Ne\ (g.s.) + e^+ + \nu_e\ (0.06\%\ of\ all\ decays)$$

and

$$^{22}Na \longrightarrow {}^{22}Ne^* + e^+ + \nu_e\ (90.4\%\ of\ all\ decays)$$

a positron and a neutrino are emitted. The ^{22}Ne ground state is stable; however, the first excited state of ^{22}Ne at 1275keV decays with a lifetime of 3.7ps in the gamma decay process

$$^{22}Ne^* \longrightarrow {}^{22}Ne_{g.s.} + \gamma_{1275}.$$

which gives rise to a characteristic gamma ray with energy 1275 keV. In both the cases, the positrons slow rapidly in the radioactive source material and disappear in the annihilation process

$$e^+ + e^- \longrightarrow 2\ \gamma\ (511\ keV\ each)\ ,$$

producing two annihilation gamma rays which share the rest mass and kinetic energy of electron and the positron. These are observed to possess approximately 511 keV of energy and have opposite momentum, thus obeying conservation laws.

(2) Electron Capture: In this decay process, an atomic electron is captured by the ^{22}Na nucleus in the reaction

$$^{22}Na + e^{-} \longrightarrow {}^{22}Ne^{*} + \nu_e \text{ (9.5\% of all decays)}$$

and a monoenergetic neutrino is emitted. The electron capture process populates only the first excited state of ^{22}Ne at 1275 keV and therefore characteristic 1275 keV gamma rays result. Annihilation gamma rays at 511 keV are not produced in electron capture because positrons are not created. [4]

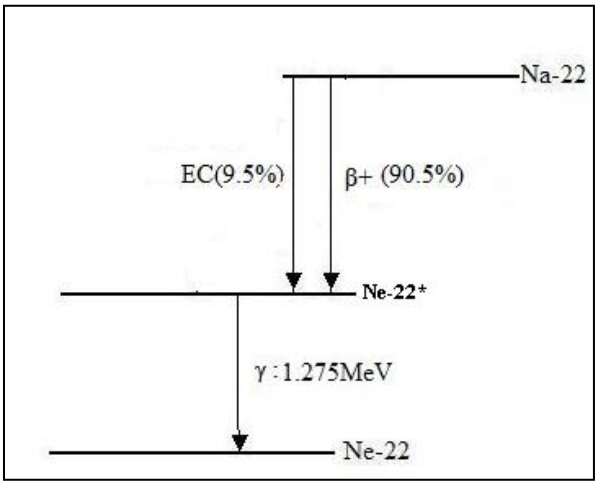

Figure 1: Decay mechanism of Na-22

Experimental Details:

The schematic set-up is shown in Fig.2.Two $LaBr_3$ crystals of diameter 1.5inches are used here. One detector is fixed at 100cm in position with respect to the source. The distance of the second detector from the source is varied from 100cm to 600cm in steps of 100cm.The γ-ray incident on a crystal can interact at any length within the crystal related to the probability of interaction, so both detectors are kept at d >100 cm from the source to ensure that $d_{1/2}$(half-thickness) << d. With a 20μCi strong source, reasonable coincidence counts (~4/sec) are obtained even at the farthest distance from the source. Both the detectors are surrounded with lead bricks to reduce the random coincidences.

It should be mentioned that the source and the first detector are not to be disturbed from their initial positions throughout the experiment. The detectors are coupled to PMTs which are biased to high voltage 850V by means of high voltage power supply (ORTEC 556).

The dynode output from both the detectors is given to spectroscopy amplifier (Mod.N968) with the gain adjusted such that 4V on an oscilloscope correspond to 511keV for both the detectors. The shaping time is kept at 2μs in both the amplifiers. The bipolar output from both the amplifiers is given to an ADC (AD913A Quad8k ADC). The energy spectrum was calibrated using both ^{22}Na and ^{60}Co.

The anode outputs from the detectors are given to constant fraction discriminators (TC 454 Quad CFD). The CFD uses the constant fraction principle to give the time of occurrence of the 511keV gamma based on the rising edge of the pulse. It outputs a fast, NIM logic pulse that is led to the TAC to trigger it. The threshold set on the CFD of detector 2 was 140keV and that for the detector 1 was 83keV.The width of the output pulses from both the CFDs is set to 200ns.

The time between the two detectors is measured by a time-to-amplitude (or pulse height) converter (TAC): that converts the time between two signals into a voltage that is proportional to the time difference between the "start" and "stop" signals into the TAC. The CFD o/p from the far detector is chosen as the start signal for the TAC and that from the fixed nearer detector as STOP signal. This is because the counting rate will be much higher in the fixed detector than in the detector that is moved, and it is better to start the TAC with the lower of the two counting rates to decrease the TAC dead time. The TAC output is given to ADC. The delay between START and STOP is adjusted to 74ns, so that the time peak in ADC is at a comfortable range for tracking changes.

Upon receiving the START signal from the second detector, the TAC begins charging a capacitor. The capacitor stops charging when the STOP signal is received from the fixed detector set to the other 511keV annihilation quanta, producing a stored charge on the capacitor proportional to the time difference. This potential discharges, sending a voltage pulse to the ADC which digitizes and records the maximum voltage. Since in Na-22 decay we also get a gamma photon of energy 1.275MeV due to de-excitation of Ne-22 to ground state, the start and stop signals from the two CFDs are given to the inputs of a coincidence logic unit (CO 4010) to get the logic $\bar{X}=\overline{\bar{A} + \bar{B}}$ .This is given to the gating input of the ADC. It is also fed to the input of a linear rate meter (Tennelac TC 527) which gives the count rate. The ADC digitizes each pulse it receives from the TAC. It stores this information across its 8192 channel range.

Data was taken in TAC range 200ns and 50ns (for better sensitivity).Each point was repeated twice and spectra were recorded in list mode using Lamps in event by event basis (T, E1, E2).To measure the time difference between the two photons TAC spectrum gated with 511keV in both the detectors are created.The gated spectra displays a "peak," the coincidence peak, whose center corresponds to the best estimate of the average time difference between the two detector signals. Due to pulse shaping effects, timing resolution of the detectors, there is be a distribution in the time differences and hence a spread in the coincidence peak. To measure the speed of light, we move the second detector and measure the shift in the location of the peak in the spectra. By calibrating the time scale, we determine the actual time the photon took to go the extra distance to reach the second detector, and thus the speed of light. The energy, ungated TAC and gated TAC spectra are shown in Figure 3, 4, 5 respectively.

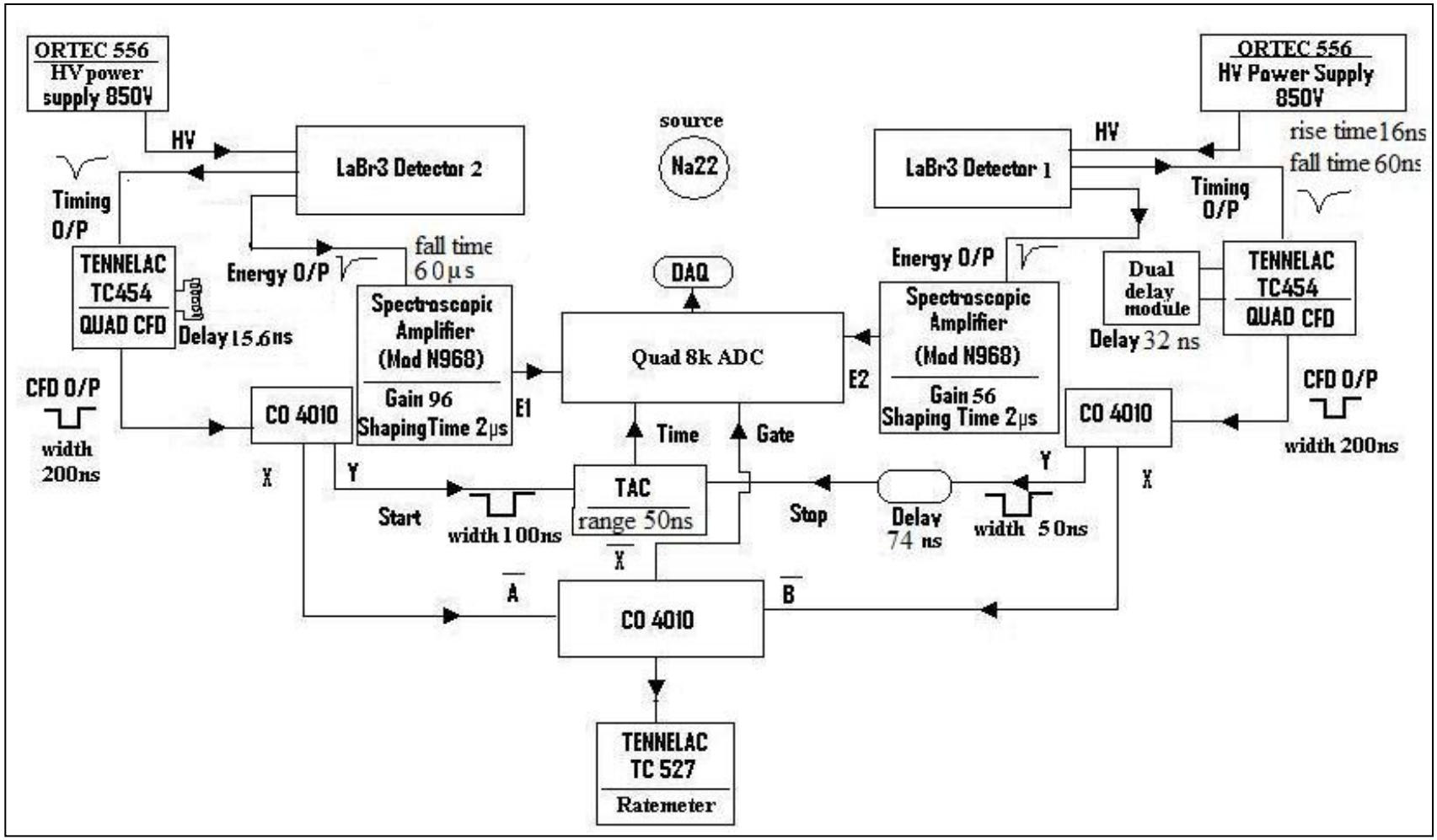

Fig.2 Block diagram of the set-up

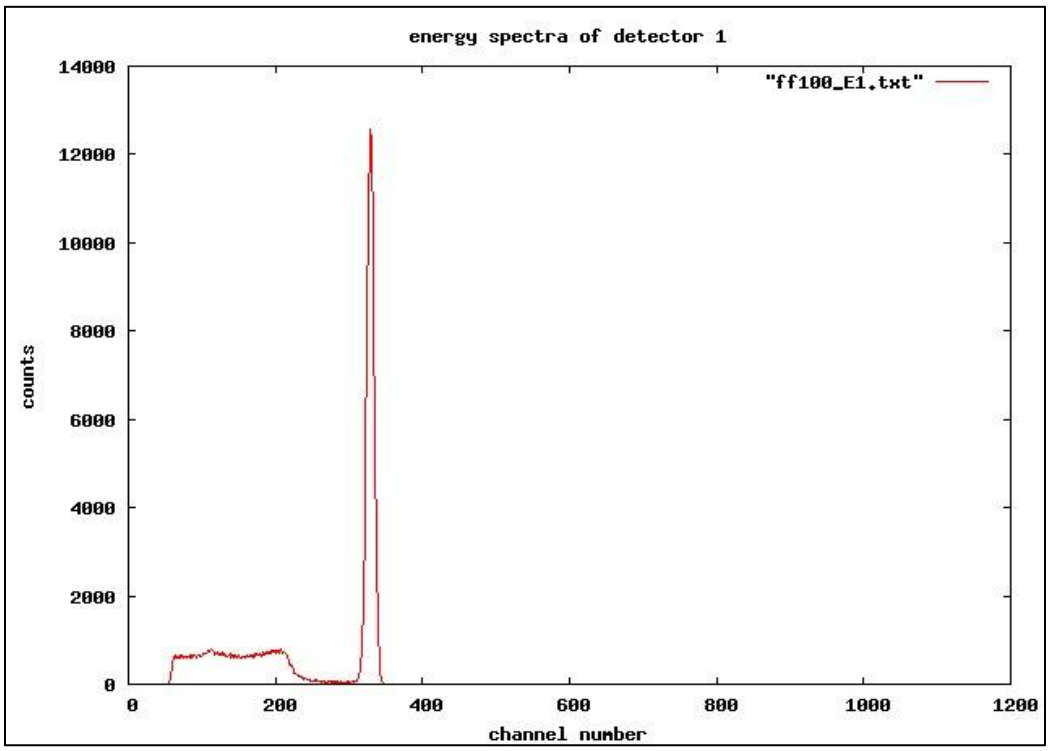

Figure3.Energy spectra of detector 1

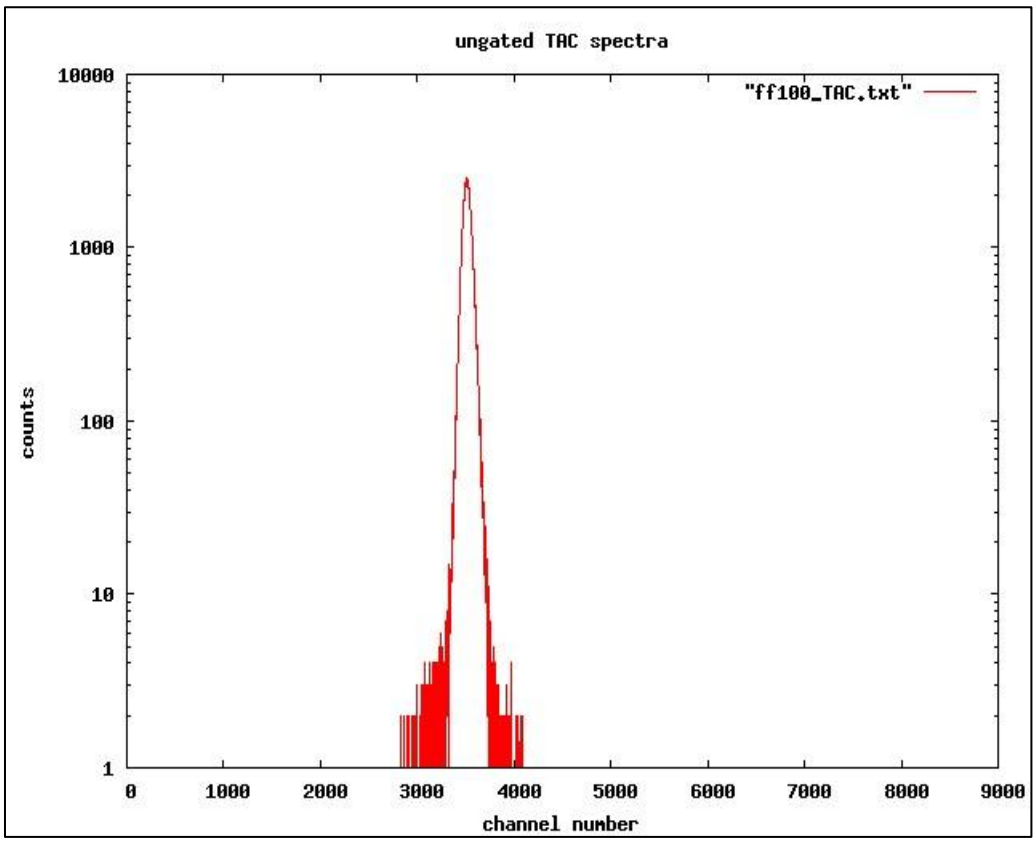

Figure 4.TAC spectra with counts in logscale

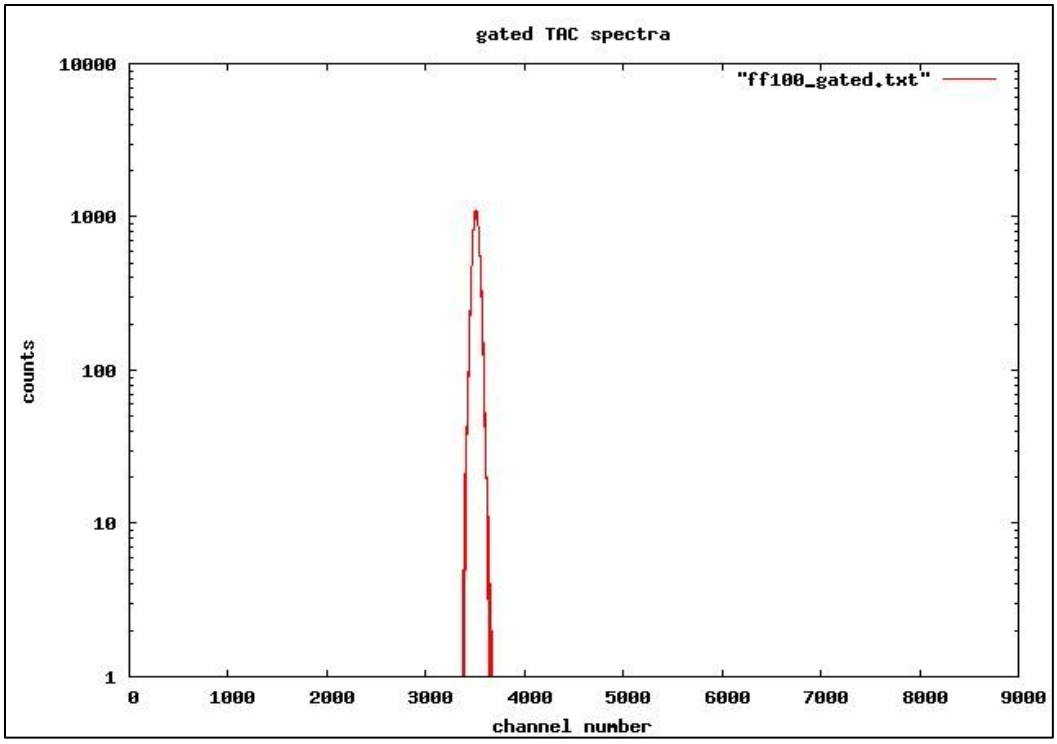

Figure 5.gated TAC spectra with counts in log scale

Time calibration:

It is first necessary to calibrate the ADC for an accurate time scale. A high precision time calibrator module (Ortec 462) is used here. The start and stop cables are connected to the TAC. The range of the calibrator is set to 80ns and the period to 10ns. Peaks are observed at an interval of 10ns.They are fitted against the respective channel numbers by the equation

$$f(x) = a*x + b \quad \ldots (1)$$

and the values obtained for a and b are as follows:

a=0.0065809±0.0000015

b=1.19504±0.00755

Calibration was done at periodic intervals (~48 hrs).

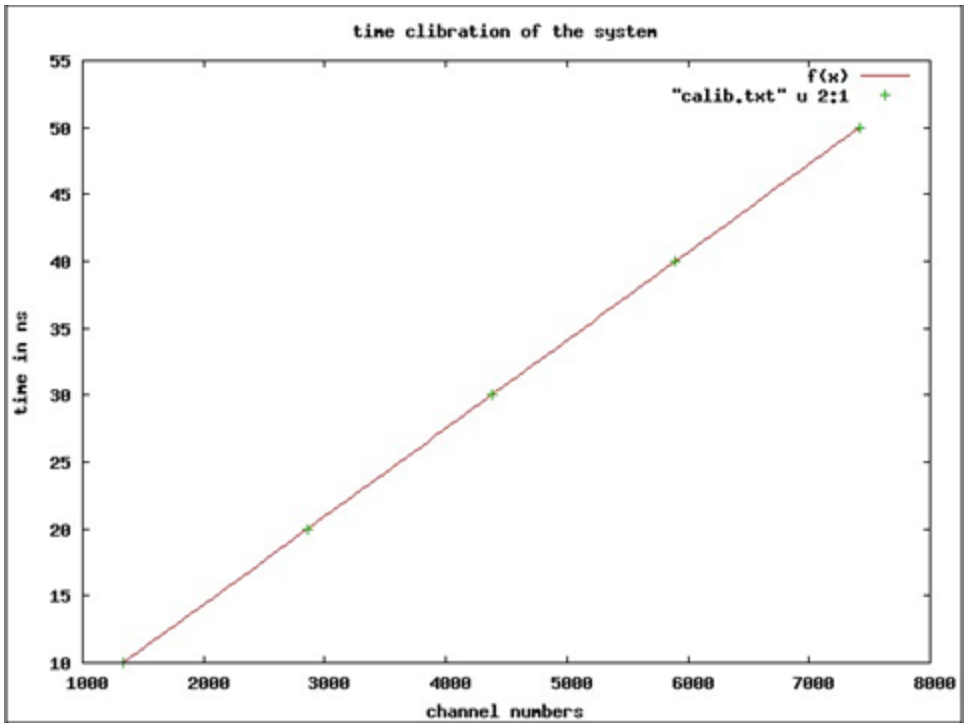

Figure 6: Graph showing the channel numbers vs. time using time calibrator

To ensure the reproducibility of the set-up the second detector was moved back again from 600cm position to 100cm and readings were taken at each intermediate positions. There was notable shift among the channel numbers which was taken care of by taking a weighted mean of the channel numbers and quoting the final error as the standard deviation of the distribution of channel numbers at a particular position.

The numerical values for distances versus the channel number are listed in Table.1 and are shown graphically in Fig.4.

Table 1.

Position of the second detector from the source (in cms)	Peak positions	Error in distance (in cms)	Error in peak positions
100	3505.39	0.1	2.309
200	2992.06	0.1	1.915
300	2486.70	0.1	2.979
400	1985.66	0.1	1.313
500	1470.94	0.1	2.907
600	971.80	0.1	1.542

The slope of distance versus channel is obtained by fitting the distance to the peak position with the function:

$$f(x)=a*(x-x_0) + b \quad \ldots (2)$$

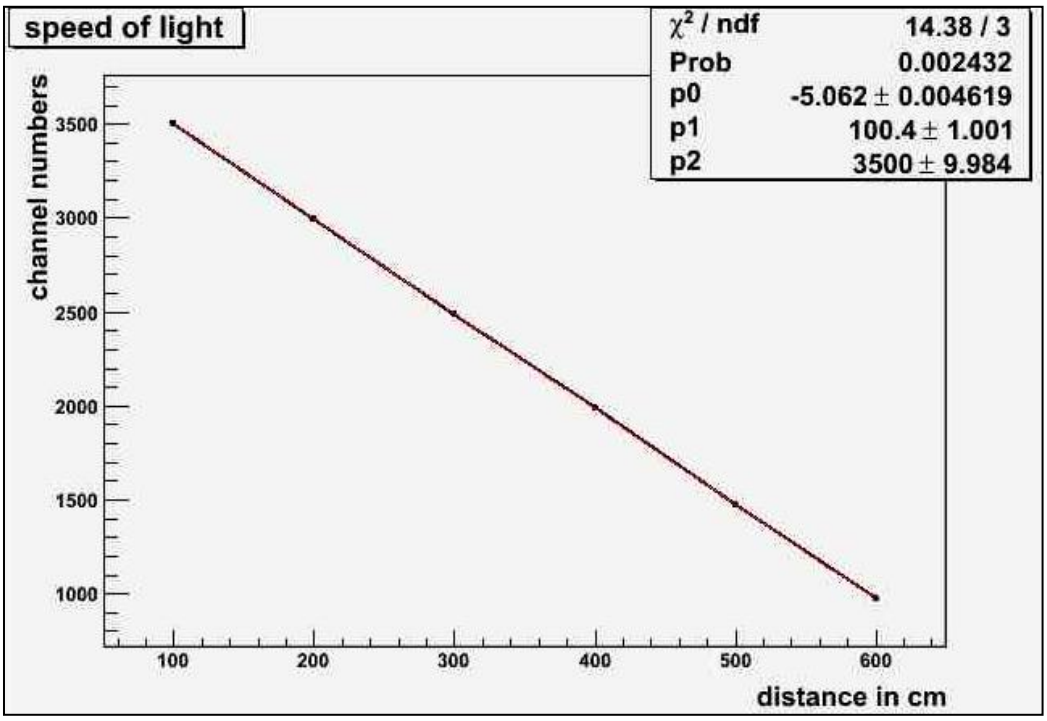

Figure 7: graph showing the channel numbers as a function of displacement of the detector 2

Sources of error:

Since this is a precision experiment, it is very essential to understand the sources of different kinds of errors and their propagation.

1. Measurement errors: Since the second detector is kept fixed at different positions and also moved back and forth with respect to one position, error of ~1mm in distance is estimated. The metre scale is verified with 75cm vernier callipers.
2. Statistical errors: To ensure good statistics, around 1,00,000 counts were taken at each position of the second detector which implied that the data at larger distances are collected in considerably long time (~ 24hours).
3. Fitting errors: All the TAC peaks are fitted with a Gaussian function but the fitting errors are very negligible (~ 10^{-5}) as compared to measurement errors (~10^{-3}) and hence the former are neglected in the subsequent analysis.
   The time calibration done using the calibrator is also fitted to a straight line and had an error ~10^{-4} which is taken into consideration.
4. Linearity of the Electronics: The drift in the characteristics of the various equipments used due temperature changes is minimised by suitable cooling of the set-up.

Results:

The slope obtained from the Fig. is 5.062 ± 0.004619 channel/cm.

Using the time calibration of the system, 0.0065809 ± 0.0000015 ns/channel we obtained the speed of light: 30.018 ± 0.028 cm/ns.

For our time calibration, we obtained a percentage error of 0.02% .The fit to the data in table1 gives us a percentage error of 0.09%.The combination of the two slopes gives us an overall error 0.09% on the value of speed of light.

Conclusions:

The speed of light is determined to be 30.018 ± 0.028cm/ns which is close to the reference value of 29.99792458cm/ns. The advantage of this experiment is that the classic experiment of "speed-of-light" can be performed on a laboratory table.

Acknowledgement:

I am highly indebted to Prof. V. Nanal for providing such a wonderful opportunity to work in the Pelletron Laboratory .She kept us motivated throughout the work. I am also thankful to Prof. R. G. Pillay for his guidance and valuable suggestions. I would like to express my sincerest gratitude to Mr. Vivek Singh and Ms. Sheetal Thakur. They were always available for discussions. It was a thoroughly enjoyable and learning experience.

References:

[1]$LaBr_3$:Ce scintillators for gamma-ray spectroscopy, Shah. K.S., Glodo. J, Wegerman. M., Moses W.W., Deremzo S.E., Weber M.J., [LBNL 2002]

[2] Comparison of $LaBr_3$:Ce and NaI(Tl) scintillators for RIID, B. D. Milbrath, Fast J. E., Kouzes R. T., Choate B. J., Hensley W. K., Schweppe J.E., [PNNL-15831]

[3]"Speed of light "measurement using BaF_2 scintillator detectors, Lee Chow, Stephen Lukacs, Kent Hopkins, [Eur. J. Phys. 15 (1994) 49-52.]

[4] http://www.nndc.bnl.gov

[5] Table of isotopes Vol.2, by Richard B.Firestone and Virgina S. Shirley

Appendix:

Calculation of half-life of a state of Sm-152:

Eu-152 disintegrates 72.1% by electron capture and about 0.027% by emission of positrons to Sm-152 and by β^- emission (27.9%) to Gd-152. [5] The same set-up is used to employ the technique of delayed $\gamma\gamma$ coincidences using a Eu-152 source. The two identical $LaBr_3$ detectors are placed close to ^{152}Eu to get high number of counts here. Lifetime of the 121keV 2^+ state in Sm-152 is measured. The 1408-121keV cascade is used. The threshold on the CFD of the latter detector is reduced to 50keV. START signal from one detector marks the occurrence of 1408keV and the STOP signal from the other detector pertains to 121keV. Hence the TAC output is gated with 1408keV and (2^+ - 0^+) 121keV energies from the respective detectors. The gated spectra have an exponential variation, characteristic of radioactive decay, following the function:

$$N=N_0*\exp(-t/\tau) \quad \ldots (3)$$

where τ is the mean-lifetime of the state.

The time calibration of this system is obtained using the time calibrator to be 0.0526592±0.0000046 ns/channel.

The graph obtained is fitted with the function:

$$f(x)=p0*\exp(-x/p1) \quad \ldots (4)$$

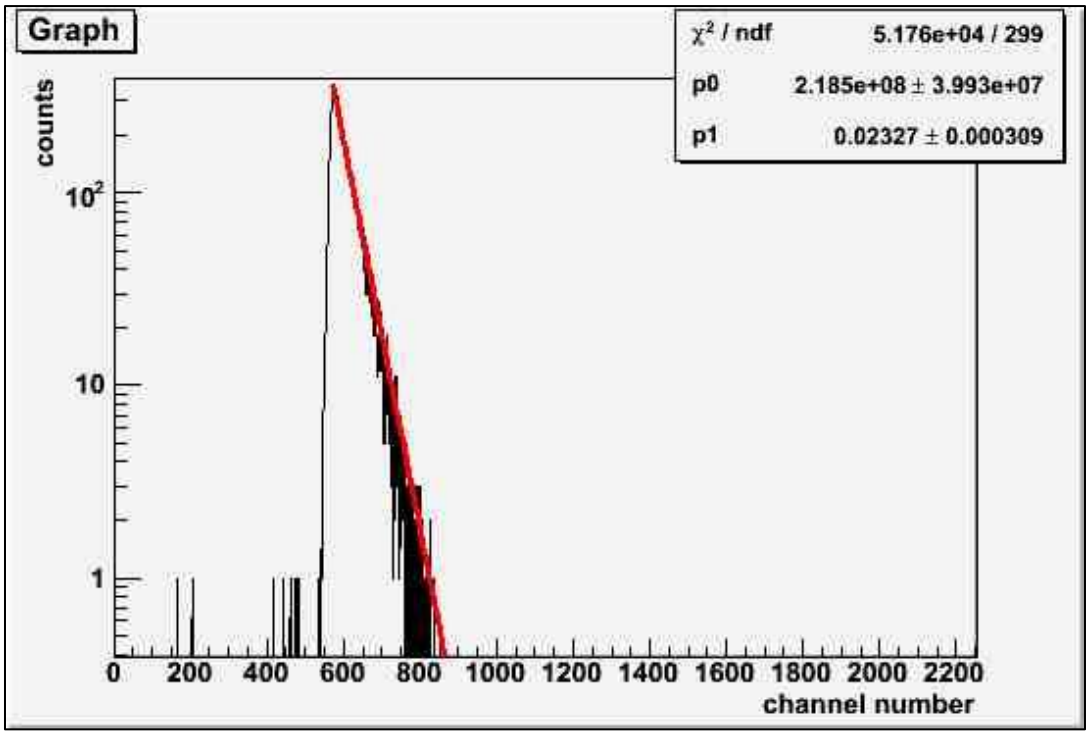

Figure 8: Fitted graph for the exponential curve of the TAC gated spectra with counts in log scale

We know that the mean-life and half-life are related as,

$$t_{1/2} = \tau \ln 2 \quad \text{... (5)}$$

Using the time calibration, the half-life of the state is obtained as:

$$t_{1/2} = 1.57 \pm 0.02 \text{ ns}$$

Experimental Project Report

on

Active Cosmic ray shield and passive shield for low background measurements with HPGe detector

Submitted by

Neha Dokania

Under the guidance of

Prof. Vandana Nanal

India based Neutrino Observatory
Tata Institute of Fundamental Research
Mumbai 400 005

[4th March 2010]

Active Cosmic ray shield and passive shield for low background measurements with HPGe detector

Abstract:

The experiment aims at the set-up of passive shielding of HPGe detector mainly against background radioactivity using lead shield and active vetoing against the cosmogenic background using a plastic scintillator in anti-coincidence arrangement with the HPGe detector. The background gamma-ray spectra were studied for both with and without lead shield and identification of various lines and their origins was done. There was suppression in background counts on using the lead shield .The veto shield showed a reduction of cosmic ray- induced count (mainly muons) in high energy region of the spectra.

Introduction:

Gamma- ray spectroscopy is used for the identification and quantification of gamma-emitting radio nuclides. The equipment used in gamma spectroscopy includes an energy-sensitive radiation detector, a pulse sorter (i.e. multichannel analyzer), and associated amplifiers and data readout devices. The most common detectors include sodium iodide (NaI) scintillation counters and high-purity germanium detectors. The choice depends on a given application. In this experiment, accurate energy determination was the prime objective. Hence, due to an excellent energy resolution and a high efficiency, HPGe detector was the obvious pick.

The background of these detectors is composed of cosmic radiation and radiation coming from the radio nuclides found around and inside the detector. In low-level counting, a variety of techniques to reduce the background has been employed and makes it possible to study an environmental sample containing a trace of gamma-emitting radio nuclides.

Sources of background:

Background radiations can be grouped as:

1. The natural radioactivity of the constituent materials of the detector itself.
2. The natural radioactivity of the equipment, supports, and shielding placed in the immediate vicinity of the detector.
3. Radiations from the activity of the earth's surface, construction materials of the laboratory, or other far-away structures.
4. Radioactivity in the air surrounding the detector.
5. The primary and secondary components of cosmic radiation.

The nature of this background varies greatly with the size and type of detector and with the extent of shielding placed that may be placed around it. [1]

High purity germanium detector:

Germanium detectors are semiconductor detectors having a p-i-n structure in which the intrinsic (i) region is sensitive to ionizing radiation, particularly x-rays and gamma rays. They behave like solid ionization chambers. Incident charged particles deposit ionization energy and dislodge electrons, which in turn produce secondary ionization. This causes a separation of the electrons and holes in the semi-conductor, which then separate due to the presence of an electric field. They collect at the electrodes, giving a signal proportional to the deposited energy. The detector has better resolution than gaseous ion chambers since the average energy required to produce an ion pair in Ge is 2.96eV at 77K, while it is typically ~30eV in gases. [2]

Because Germanium has a small band gap (0.746eV at 0K, 0.73eV at 77K), the HPGe detector was cooled with liquid N_2 (77K) to reduce the thermally-induced leakage current, otherwise the associated noise will spoil its excellent energy resolution. The detector is mounted in a vacuum chamber which is attached to an LN_2 Dewar .The detector used here was of close-ended coaxial configuration with diameter 5cm and length 7.5cm (BRUKER Serial. No. -1311-08).It was biased using HV supply (ORTEC 459) to 2400V.

Calibration of HPGe:

The raw pulse (negative) from the HPGe has a rise time of 0.8μs and pulse height of 500mV.

The energy signal from the detector is fed to a spectroscopy amplifier (Mod. N968).After amplification, the signal is given to an 8K ADC (CM F48 Quad. NADC).The gain of the amplifier is adjusted to 9.8 such that the 8K channels of the ADC correspond to 3MeV.

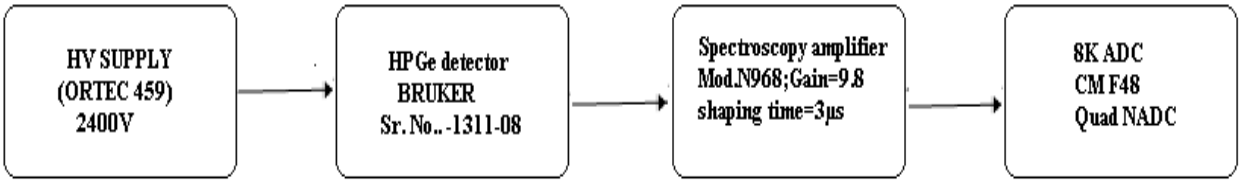

Figure1: Block diagram for calibration of HPGe

For proper identification of peaks in background spectra, the pulse height scale must be calibrated in terms of absolute gamma-ray energy. Standard sources like Co-60, Eu-152 and Cs-137 are used here.

The energy lines of the spectra obtained are combined to get a calibration. The energy of known lines and the corresponding channel numbers are fitted with a quadratic function as:

$$f(x) = ax^2 + bx + c \quad \ldots (1)$$

The resolution of the detector was calculated at different energies as,

$$\epsilon = \frac{\sigma}{E}$$

where ϵ = resolution of the detector at energy E,

σ = FWHM for the peak at energy E.

and fitted with energy by the function:

$$f(x) = \frac{a}{\sqrt{x}} + b \quad \ldots (2)$$

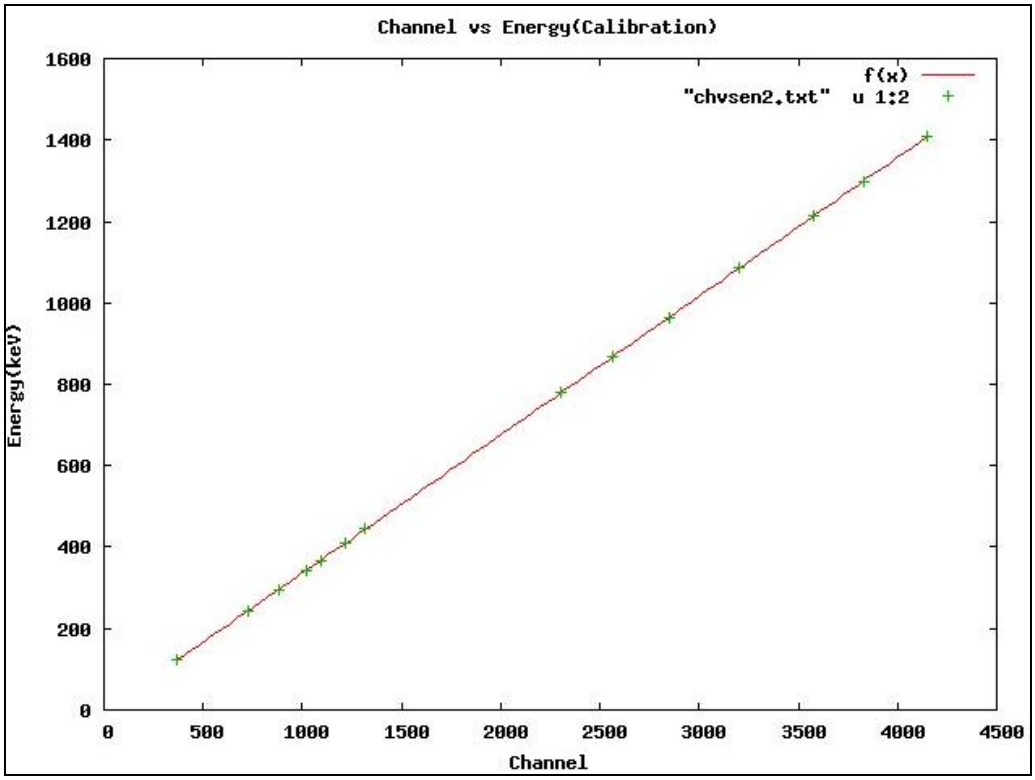

Figure2: Graph for the calibration of HPGe detector

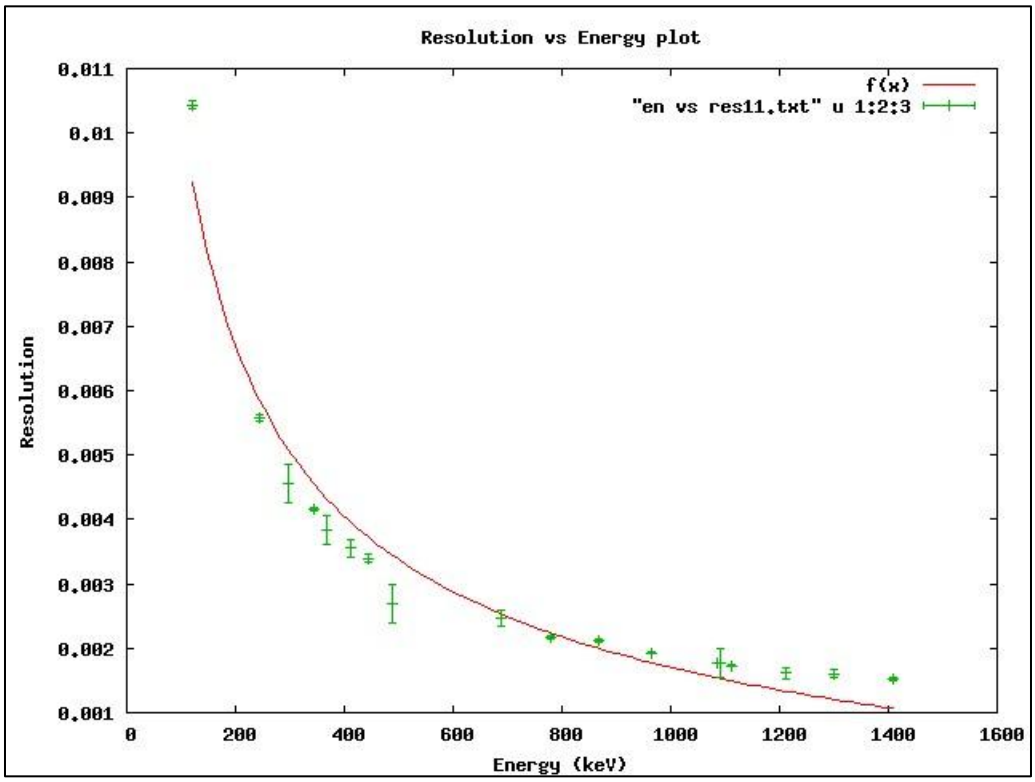

Figure3: Graph showing variation of resolution of detector with energy

Figure.3 clearly indicates that the resolution improves for the detector at higher energies.

The relative efficiency can be calculated as:

Relative efficiency $= \frac{\epsilon_{abs}^{1}}{\epsilon_{abs}^{2}} = \frac{A_1}{A_2}\frac{\gamma_1}{\gamma_2}$ where, A_1 and A_2 are the areas under the peaks at energies E_1 and E_2 respectively, and γ is the branching ratio.

The relative efficiency is plotted against energy and fitted with function as:

$$f(x) = \frac{a}{x^2} + \frac{b}{x} + c \quad \ldots (3)$$

Table 1: Relative efficiency and resolution of the HPGe detector at different energies

Energy (keV)	**FWHM (keV)**	**Branching ratio (%)**	**Counts**	**Resolution (FWHM/energy)**	**Rel. eff. (w.r.t 121.8keV)**
121.8 ± 0.004	1.27 ± 0.01	28.37	107949 ± 1054	0.010437 ± 6.5e-05	1.00 ± 0.01
244.7 ± 0.005	1.36 ± 0.01	7.53	20927 ± 246	0.005571 ± 4.5e-05	0.73 ± 0.01
295.9 ± 0.032	1.35 ± 0.09	-	1054 ± 87	0.004552 ± 0.000294	-
344.3 ± 0.004	1.43 ± 0.01	26.57	55740 ± 511	0.004153 ± 2.3e-05	0.55 ± 0.01
367.8 ± 0.028	1.41 ± 0.08	-	1723 ± 121	0.003836 ± 0.000215	-
411.1 ± 0.02	1.46 ± 0.06	2.238	4036 ± 195	0.003556 ± 0.000136	0.47 ± 0.02
443.9 ± 0.01	1.51 ± 0.03	3.125	5457 ± 124	0.003396 ± 5.8e-05	0.46 ± 0.01
488.8 ± 0.057	1.32 ± 0.15	-	559 ± 83	0.002692 ± 0.000307	-
688.7 ± 0.031	1.70 ± 0.08	-	1069 ± 68	0.002468 ± 0.000115	-
778.9 ± 0.009	1.69 ± 0.02	12.97	13482 ± 251	0.002179 ± 2.6e-05	0.27 ± 0.06
867.4 ± 0.011	1.84 ± 0.03	4.214	4356 ± 94	0.002118 ± 3.59e-05	0.27 ± 0.01
964.1 ± 0.008	1.86 ± 0.02	14.63	13043 ± 183	0.001930 ± 1.8e-05	0.23 ± 0.07
1085.9 ± 0.012	1.93 ± 0.01	10.13	586 ± 62	0.001799 ± 0.000147	0.15 ± 0.05
1089.8 ± 0.035	1.92 ± 0.24	1.731	8231 ± 136	0.001776 ± 1.9e-08	0.29 ± 0.03
1112.1 ± 0.008	1.93 ± 0.02	13.54	1476 ± 67	0.001769 ± 0.000220	0.28 ± 0.02
1212.9 ± 0.039	1.96 ± 0.11	1.412	1083 ± 146	0.001732 ± 1.4e-05	0.21 ± 0.03
1299.2 ± 0.034	2.08 ± 0.09	1.626	1053 ± 75	0.001618 ± 8.9e-05	0.19 ± 0.02
1408.0 ± 0.01	2.15 ± 0.02	20.85	1180 ± 66	0.001604 ± 6.6e-05	0.19 ± 0.01
			13680 ± 228	0.001524 ± 1.4e-05	0.17 ± 0.02

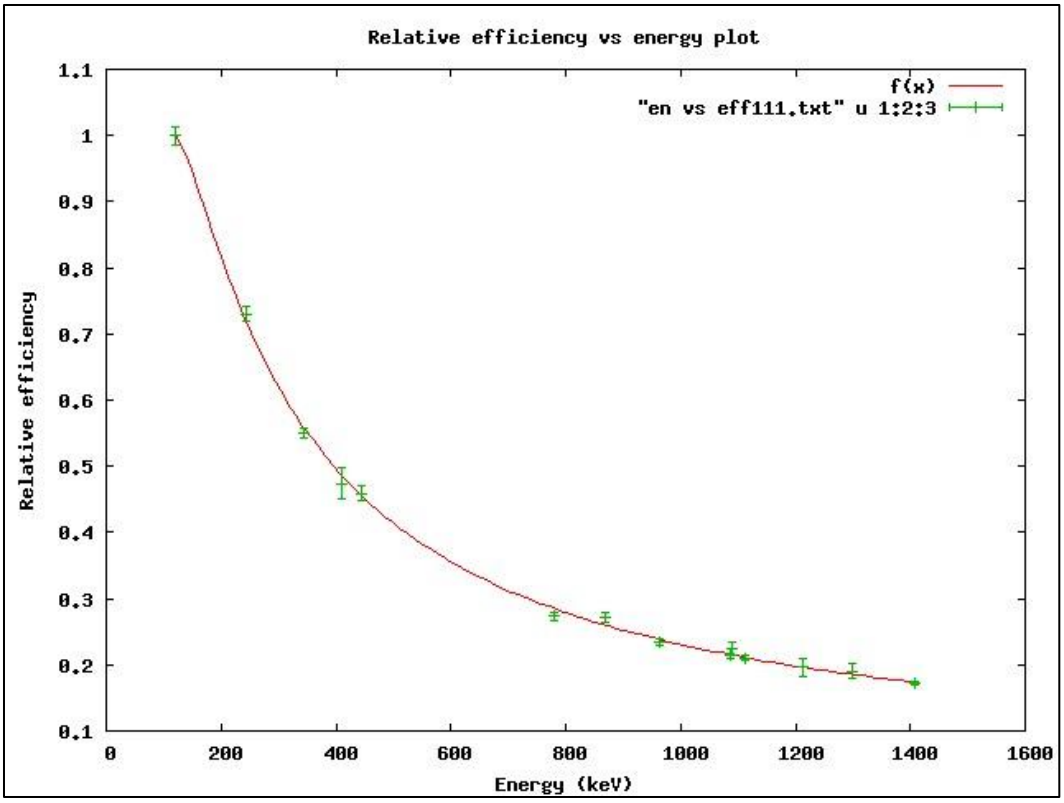

Figure4: Graph showing variation of relative efficiency of the detector with energy

The data is not dominated by statistical fluctuations as seen from Figure 4.but by fluctuations due to electrical noise, etc.

Background spectrum and its identification:

The radioactivity of ordinary construction materials is, in large part, due to low concentrations of naturally radioactive elements often contained as an impurity. The most important components are potassium, thorium and uranium, and the members of the long decay chains of uranium and thorium.

The background spectrum in the range 0-3MeV is recorded for 12 hours after removing all the sources from the laboratory. Using the calibration obtained, the following lines are identified from the known background data. [3] [4]

The following daughter activities are identified: in the thorium series, ^{228}Ac, ^{224}Ra, ^{212}Bi, ^{212}Pb, and ^{208}Tl; in the uranium series, ^{226}Ra, ^{214}Pb, and ^{214}Bi.The long-lived activities of ^{235}U and ^{40}K are also evident. Common materials used in the construction of detector systems such as aluminium, stainless steel contain potassium, thorium, and/or uranium as a normal constituent and therefore have a rather high background level.

No lines were observed for ^{60}Co (1.17MeV and 1.33MeV),since this experiment was carried in counting room on ground floor of pelletron building , which were actually evident when the experiment was done in the first floor of the same building. However lines due to ^{137}Cs (0.661MeV) were identified in the spectrum, clearly showing the effect of the surrounding structural materials on the background.

Table 2: Background lines and their respective sources

Calibrated Energy(keV)	Source	Exact energy(keV)	Calibrated Energy(keV)	Source	Exact energy(keV)
185.8	^{235}U,^{226}Ra	185.7,186.2	860.6	^{208}Tl	860.6
209.1	^{228}Ac	209.3	911.1	^{228}Ac	911.2
238.4	^{212}Pb	238.6	934.1	^{214}Bi	934.1
241.8	^{224}Ra,^{214}Pb	240.9,241.9	964.7	^{228}Ac	964.8
270.1	^{228}Ac	270.2	968.9	^{228}Ac	969.0
277.1	^{208}Tl	277.4	1120.3	^{214}Bi	1120.3
295.1	^{214}Pb	295.2	1238.2	^{214}Bi	1238.1
300.1	^{212}Pb	300.1	1281.1	^{214}Bi	1280.9
327.7	^{228}Ac	328.0	1377.9	^{214}Bi	1377.7
338.2	^{228}Ac	338.3	1384.9	^{214}Bi	1385.3
351.8	^{214}Pb	351.9	1401.4	^{214}Bi	1401.5
409.3	^{228}Ac	409.5	1408.1	^{214}Bi	1407.9
462.9	^{228}Ac	463.0	1460.8	^{40}K	1460.8
510.8	^{208}Tl,^{40}K	510.8,511.0	1495.9	^{228}Ac	1495.9
583.1	^{208}Tl	583.2	1501.8	^{228}Ac	1501.6
609.3	^{214}Bi	609.3	1587.9	^{228}Ac	1588.5
661.6	^{137}Cs	661.7	1592.3	^{208}Tl DE	1592.5
665.6	^{214}Bi	665.4	1620.8	^{212}Bi	1621.0
727.3	^{212}Bi	727.2	1630.6	^{228}Ac	1630.6
762.2	^{208}Tl	763.1	1661.2	^{214}Bi	1661.3
768.3	^{214}Bi	768.4	1729.7	^{214}Bi	1729.6
772.4	^{228}Ac	772.3	1764.5	^{214}Bi	1764.5
785.7	^{214}Bi	786.4	1847.5	^{214}Bi	1847.4
794.9	^{228}Ac	794.9	2103.5	^{208}Tl SE	2103.5
806.4	^{214}Bi	806.2	2118.2	^{214}Bi	2118.5
830.6	^{228}Ac	830.5	2204.1	^{214}Bi	2204.1
835.6	^{228}Ac	835.7	2447.8	^{214}Bi	2447.7
839.9	^{228}Ac	840.4	2614.4	^{208}Tl	2614.5

Passive Shielding:

The magnitude of background due to natural radioactivity can be considerably reduced by means of passive shielding. Because of high density (11.34 g/cm^3) and large atomic number (Z=82), lead is the most widely used material for the construction of detector shields. The energies of gamma rays produced by the natural radioactivity are limited to about 3MeV, and gamma rays with these energies are effectively attenuated with about 10cm thick lead shield.

A lead house of thickness 5cm is built around the HPGe detector .The background spectra is recorded with the passive shielding for 36 hours and the reduction in the counts per hour is calculated, as shown in the table below:

Table 3: Reduction in background after passive shielding

Energy(keV)	Counts/hr without lead house (X)	Counts/hr with lead house (Y)	Reduction in counts (X/Y)
74.9	162.8 ± 66.0	52.3 ± 2.5	3.1 ± 1.3
92.4	155.8 ± 35.5	30.0 ± 1.8	5.2 ± 1.2
185.8	216.2 ± 31.2	25.6 ± 2.4	8.5 ± 1.5
238.4	1520.2 ± 218.2	26.2 ± 3.8	58.1 ± 11.9
351.8	758.7 ± 20.0	8.2 ± 2.7	92.9 ± 30.4
510.8	346.0 ± 19.2	62.1 ± 4.4	5.6 ± 0.5
583.1	615.0 ± 20.1	8.7 ± 1.7	70.7 ± 14.2
609.3	795.3 ± 20.8	8.4 ± 1.7	94.2 ± 19.1
661.6	101.7 ± 9.4	69.9 ± 2.2	1.5 ± 0.1
911.1	543.2 ± 12.7	5.9 ± 1.9	91.8 ± 30.3
968.9	277.5 ± 9.3	4.9 ± 1.5	56.1 ± 17.4
1120.3	224.8 ± 8.0	6.4 ± 0.4	34.9 ± 2.7
1460.8	2342.4 ± 30.5	79.1 ± 1.9	29.6 ± 0.8
1592.3	64.0 ± 2.3	4.2 ± 2.6	15.4 ± 9.6
1764.5	220.9 ± 8.1	17.1 ± 5.8	12.9 ± 4.4
2614.4	514.6 ± 9.8	31.2 ± 1.8	16.5 ± 1.0

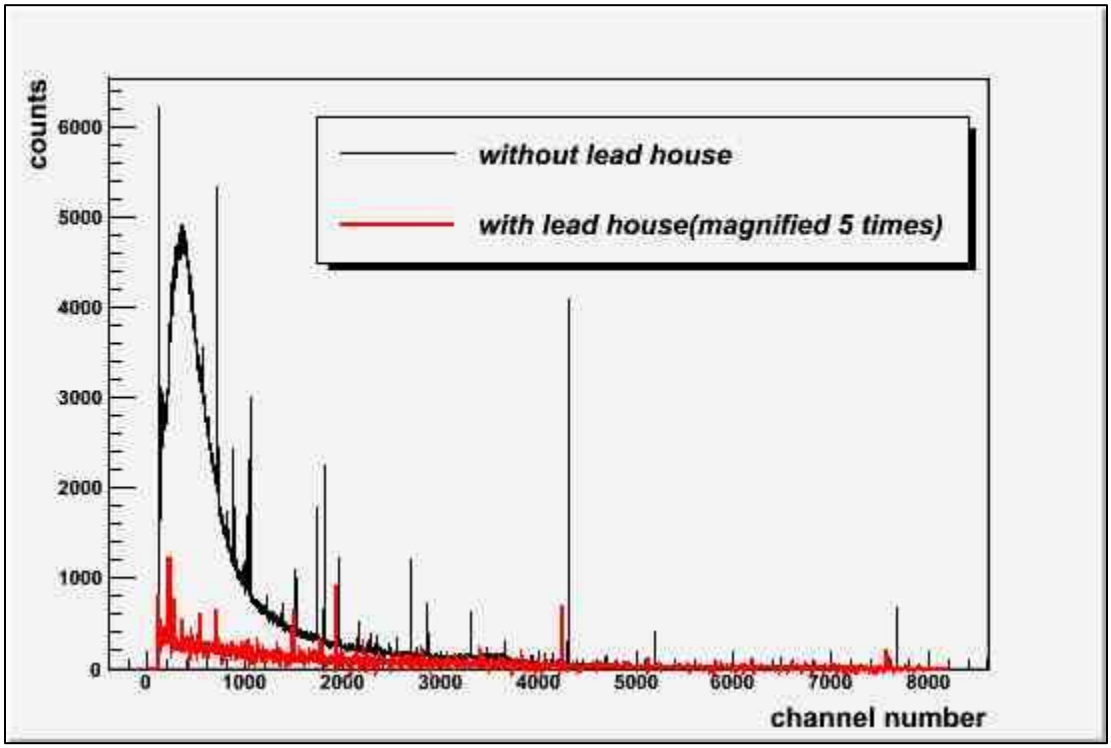

Figure 5: Background spectra for 12hours without and with shielding

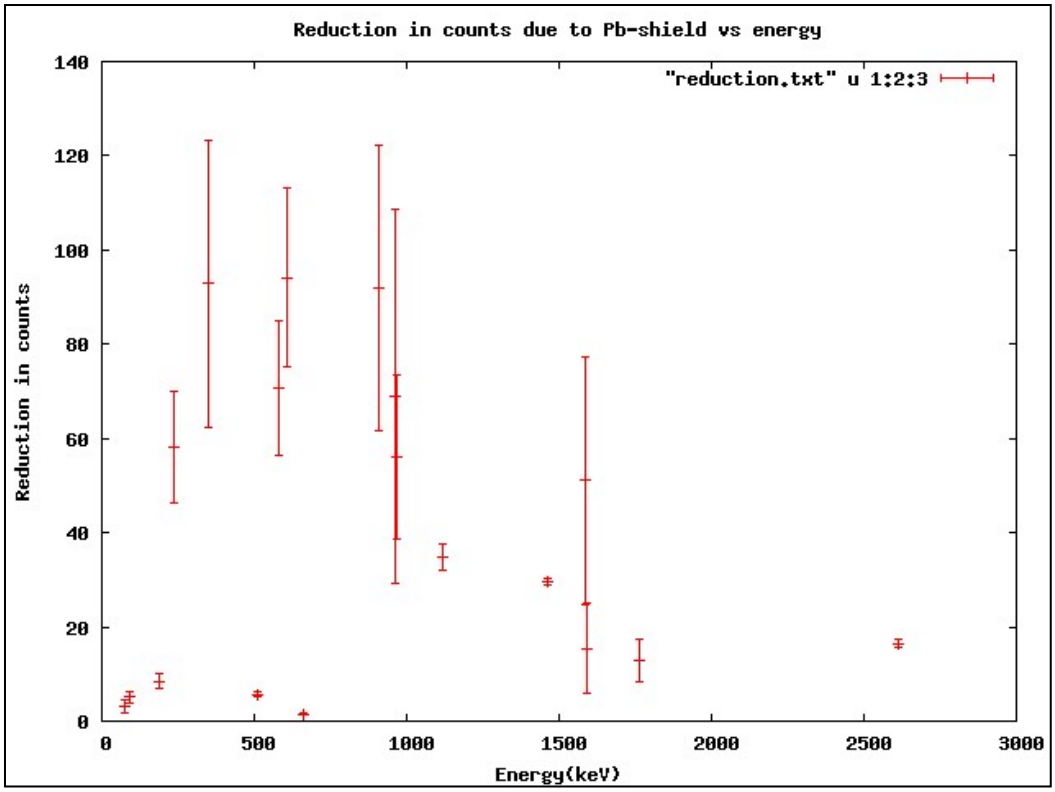

Figure6: Reduction in counts due to lead shielding at different energies

Figure6.shows that the counts at lower energies (74.9 keV and 92.4keV) are not reduced greatly as these correspond to lead X-rays. The reduction in counts also decreases at higher energies.

The intensity of a parallel beam of photons passing through an absorber of thickness d decreases as,

$$I = I_0 2^{\frac{-d}{d_{1/2}}} \quad \ldots(4)$$

For lead, the half- thickness at photon energy 2.5MeV is, $d_{1/2}$=1.3cm.[5]

From table.3, at 2.6MeV $\frac{I_0}{I} = 16.5 \pm 1.0$

From equation (4), the effective thickness of lead shield is, d= (5.3 ± 0.1) cm.

Since the lead shield is not uniform from all sides and the gamma ray may pass at such an angle that they traverse greater distance in lead, the effective thickness can be greater than 5cm.

Active cosmic-ray Shielding:

To reduce the background due to highly penetrating cosmic radiations in the higher energy range, large amount of conventional shielding will be required. Hence this is accomplished through the use of an anti-coincidence shield or veto.

A plastic scintillator of dimensions 41cm x41cm x 9 cm is placed on top of the detector. The output of the HPGe detector is accepted only when it is not accompanied by a coincident pulse in the scintillator. It is assumed that the cosmic rays, primarily muons, strike the scintillator only vertically downwards.

The PMT of the scintillator is biased to 2kV by high voltage supply (ORTEC 556) .The raw pulse (negative) from the timing output of the scintillator has a rise time of 6ns and pulse height of 1V. No TFA

(Timing Filter Amplifier) is used for the scintillator signal. The timing signal is directly given to a CFD (TC 455 Quad CFD).Delay of 2.3ns was provided by a 45cm long LEMO cable to the signal.
The timing signal from the HPGe detector is given to a TFA (ORETEC 474) and then to the CFD. Delay of 64ns is given to the signal by delay unit (Dual delay module 792).Now both the timing signals are given to inputs A and B of a 4-fold coincidence logic unit(CO 4010) respectively. The Boolean logic used here is $\overline{A + \overline{B}} = \bar{A}.B$. The output of the logic unit is given to the master gate of the same ADC used before.
The energy signal from the HPGe detector is given to a different amplifier (TENNELAC TC 244) this time, whose gain is adjusted to 2.8 such that the 8k channels of ADC now correspond to 16.6MeV.

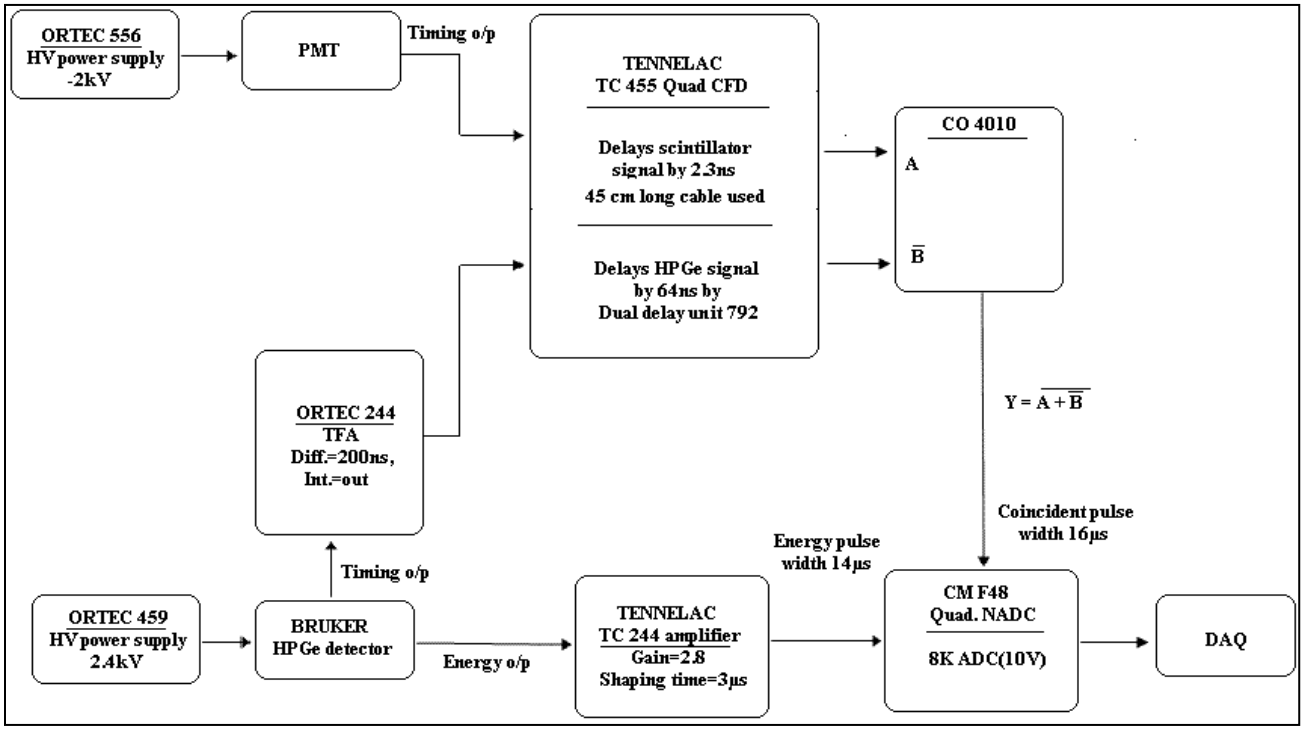

Figure7: Block diagram for Anti-coincidence set-up

Care is taken that the energy pulse is contained within the coincident pulse width. Hence the necessary arrangements are made in the width of the o/p Y in CO-4010 Logic unit.
The background spectra are recorded with the veto shield for about 74.4 hours and without veto shield for about 18hours.The reduction in counts per hour is calculated in the high energy range of the spectra.

Table 4: Reduction in background after active shielding

Energy	Counts/hr with veto (X)	Counts/hr without veto (Y)	Reduction (Y/X)
1461KeV	77.3 ± 0.7	74.3 ± 4.2	0.96 ± 0.06
2615KeV	33.0 ± 0.9	30.5 ± 1.7	0.92 ± 0.07
5-10MeV	57.2 ± 0.9	205.2 ± 3.4	3.59 ± 0.01
10-13MeV	28.1 ± 0.6	118.2 ± 2.6	4.21 ± 0.03
13-16MeV	25.6 ± 0.6	107.7 ± 2.4	4.21 ± 0.03

Hence we see that the reduction in cosmic background is better in 10-16MeV energy range than in 5-10MeV range whereas the 1461keV and 2615keV lines are not much affected as their origins lie in natural radioactivity sources which are also present as radioactive contamination (thorium) in the lead shield around the HPGe detector.

Calculation of energy deposited by muon:

The average energy of muon at sea level is 4GeV and its flux is 1muon/cm^2/min. Being a minimum ionizing particle, muon can travel substantial lengths (~ some metres) in lead. The numerical value of minimum energy loss of a minimum ionizing particle passing through matter is about 2MeV/gm/cm^2.[1] Hence, the energy deposited by muons in a particle detector can be given by:

$$E = \rho . t . \Delta E \quad \ldots (5)$$

where, ρ is the density of the material of the detector,
t is the thickness of the detector, and
Δ E is the energy lost per unit mass thickness of the detector

(a) For plastic scintillator:

$\rho = 1.05 g/cm^3$, t = 9cm, $\Delta E = 2 MeV/gm/cm^2$

From equation (5), energy deposited in the scintillator is E = 18.9MeV

(b) For HPGe detector:

$\rho = 5.32 g/cm^3$, t = 5cm, $\Delta E = 2 MeV/gm/cm^2$

Considering the vertical muons only, maximum energy will be deposited while passing through the diameter of the detector.

From equation (5), energy deposited in the HPGe detector is E = 53.23MeV.

But 16MeV muons are detected in the experiment which corresponds to those muons which pass at an angle (not vertical) to the detector, thereby covering a smaller distance than 5cm.

The thickness of the crystal at which 16MeV muons are detected can be calculated as,

$$t = \frac{5}{53.23} \times 16 \text{ cm} = 1.5 \text{cm}.$$

Conclusions:

A passive shielding of thickness 5cm using lead is built for HPGe detector and the reduction in background up to energies of 3MeV is noted. The origins of the background lines are identified and the effect of structural contaminants of the surrounding is also appreciated. An active veto shield using plastic scintillator is then set up with the HPGe detector to reduce the cosmogenic background up to 16MeV, which works effectively. Thus we looked into the techniques of reduction of background for a detector, which is very crucial in experiments involving sources of low activity and in rare event searches like neutrino-less double beta-decay.

Acknowledgement:
I am highly indebted to Prof.V.Nanal for providing such a wonderful opportunity to work in the Pelletron Laboratory .She kept us motivated throughout the work. I am also thankful to Prof. R.G.Pillay for his guidance and valuable suggestions. I would like to express my sincerest gratitude to Mr. Vivek Singh and Ms. Sheetal Thakur. They were always available for discussions. Lastly, I would like to thank my colleagues Moonmoon, Mathi and Animesh for their full support and co-operation. It was a thoroughly enjoyable and learning experience.

References:

[1] Radiation detection and measurement, by Glenn. F. Knoll.
[2] Introduction to experimental particle physics, by R.C.Fernow.
[3] www.nndc.bnl.gov
[4] Table of isotopes Vol.2, by Richard B.Firestone and Virgina S. Shirley
[5] E.Storm and H.I.Israel, Nucl. Data Tables A7, 565(1970).